This is a pre-copyedited, author-produced PDF of an article accepted for publication in Journal of Petrology *following peer review. The version of record* P. Špaček, L. Ackerman, G. Habler, R. Abart, and J. Ulrych: Garnet Breakdown, Symplectite Formation and Melting in Basanite-hosted Peridotite Xenoliths from Zinst (Bavaria, Bohemian Massif) J. Petrology (2013) 54 (8): 1691-1723 first published online May 31, 2013 doi:10.1093/petrology/egt028 *is available online at:* **http://petrology.oxfordjournals.org/content/54/8/1691**

GARNET BREAKDOWN, SYMPLECTITE FORMATION AND MELTING IN BASANITE-HOSTED PERIDOTITE XENOLITHS FROM ZINST (BAVARIA, BOHEMIAN MASSIF)

Petr Špaček, Lukáš Ackerman, Gerlinde Habler, Rainer Abart and Jaromír Ulrych

Abstract

Complex, symplectite-bearing pseudomorphs after garnet recently found in unique basanite-hosted peridotite xenoliths from Zinst, Bavaria, allow the study of the interaction between garnet peridotite and melts/fluids both prior to entrainment of the xenoliths and during their ascent. Based on microstructures and crystallographic fabric, major and trace element mineral chemistry, four distinct concentric zones were defined in various types of pseudomorphs:

I) coarse grained (≤ 1 mm) aggregate of orthopyroxene+clinopyroxene+spinel with a granular structure,

II) fine- to medium grained (order of 10-100 μm) orthopyroxene+spinel symplectite,

III) fine grained (5- 300 μm), radially fibrous orthopyroxene+spinel symplectite with interstitial anorthite, and,

IV) ultrafine grained (≤ 1 μm) orthopyroxene+spinel+anorthite symplectite with an internal domain sub-structure.

Zones III and IV have bulk compositions of pyrope rich garnet. All zones exhibit perfect inter-sample correlation and document the discontinuous evolution of peridotite under changing conditions with successively increasing rates of garnet breakdown.

Based on thermometry and microstructural relations, a sequence of three pre- and syn-volcanic events is discerned:

The first traceable event corresponds to regional heating in the uppermost mantle probably related to the early stages of Tertiary rifting, which triggered the reaction between garnet and olivine (Zone I) leading to a partial re-equilibration of the rock at 1040-1080°C within the spinel peridotite stability field. Subsequently a short period of heating by ~100-250°C lead to largely isochemical, fluid-mediated in situ melting of garnet and to the formation of kelyphite by crystallization from the melt (Zone III). The subsequent metasomatic alteration by external, Na-rich, K-poor, carbonate-bearing melts/fluids suggests that this phase of garnet breakdown occured largely prior to formation of the xenolith, preceding the emplacement of the basanite magma.

Finally, after xenolith formation, and associated with the rapid, isochemical, decompression during ascent, the garnet relics were transformed into microsymplectite (Zone IV). The positive volume change associated with this reaction caused fracturing, producing radial cracks that emanate from Zone IV and extend into the adjacent peridotite allowing infiltration of basanite-derived melt components.

The well developed and clearly separated symplectite zones indicating the isochemical breakdown of garnet are uncommon to garnet peridotites worldwide. Their existence at Zinst is explained by an extremely short time span between the formation of the kelyphite, Na-carbonate metasomatism and the final garnet breakdown on the basanite eruption, allowing for rapid quenching of the multiple advancing reaction fronts.

This is a pre-copyedited, author-produced PDF of an article accepted for publication in Journal of Petrology *following peer review. The version of record* P. Špaček, L. Ackerman, G. Habler, R. Abart, and J. Ulrych: Garnet Breakdown, Symplectite Formation and Melting in Basanite-hosted Peridotite Xenoliths from Zinst (Bavaria, Bohemian Massif) J. Petrology (2013) 54 (8): 1691-1723 first published online May 31, 2013 doi:10.1093/petrology/egt028 *is available online at:* **http://petrology.oxfordjournals.org/content/54/8/1691**

1. INTRODUCTION

Reaction coronae around garnet are commonly found in garnetiferous mafic and ultramafic rocks of the upper mantle and lower crustal origin. The importance of these features lies in the fact that they record retrograde metamorphism and carry information on pressure-temperature (P-T) paths or exhumation rates of the host rocks, bearing serious implications for their tectonic evolution. For this reason garnet coronae have been studied by many geologists both in rocks exposed in deeply eroded orogens (Obata, 1994; Godard & Martin, 2000 and references therein) or sampled as xenoliths brought to surface by primitive volcanic magmas (Reid & Dawson, 1972; Mukopadhyay, 1991; Keankeo et al., 2000; Dégi, 2010). Although the mineralogy and microstructure of coronae may be specific for different rocks, their basic features are often common for xenoliths and alpine-type rocks, suggesting similar mechanisms by which they are formed (e.g., Obata, 2011).

While garnet peridotite is the most common member of xenolith suites in kimberlites, it is generally very rare in alkali basalts and typically absent in most occurences of basalts worldwide. Taking into account the generally accepted assumption that garnet peridotite is a source rock for basaltic magmas, this fact probably reflects some important changes in the style of magma transport taking place close to the garnet/spinel peridotite transition. It is therefore desirable to understand the interactions between garnet peridotite and basaltic melt, since these can play an important role in chamber formation and thus control the transport of magma to shallower levels in the lithosphere. Both local advective heating and introduction of reactive fluids from the rising melts very likely destabilise the mineral assemblage in garnet peridotite. The rapidly exhumed and cooled xenoliths of garnet peridotites can bear numerous fingerprints of such late transformation processes in the sub-volcanic mantle, allowing for backward reconstruction of the physico-chemical conditions at which they occurred.

Peridotite xenoliths in basalts often contain coarse grained intergrowths of pyroxenes and spinel, which are usually interpreted as the products of olivine+garnet reaction due to static decompression or heating in the mantle. Such features are commonly found in xenoliths from the Bohemian Massif, however, these are always completely re-equilibrated with the host peridotite in the spinel stability field and their relation to the magmatic process is not clear. Garnet peridotite xenoliths have never been found in basalts of the Bohemian Massif (except for fragments derived from the alpine-type perdiotite incorporated in the crust), and in Europe only one rare occurrence was reported from the French Massif Central (Cheval et al., 1989).

Recently, we found rare xenoliths in basanite from Zinst (Bavaria, Germany) containing zoned mineral clusters with fine grained symplectites, representing former garnet and its reaction coronae. The chemical and textural evidence clearly shows a multiphase breakdown of garnet which was not completed before the entrainment of xenoliths into basanites, and hence likely records the processes taking place in the upper mantle prior to eruption. Although generally similar in appearance to reaction coronae commonly observed in garnet peridotites, these pseudomorphs exhibit some features not described earlier in the literature, indicating at least three phases of garnet decomposition, including both reaction with olivine and isochemical breakdown. The xenoliths from Zinst provide a unique opportunity to study in unusual detail the processes of garnet breakdown in peridotite and the formation of fine grained symplectites. In the present paper we give a comprehensive description of mineralogical, chemical and microstructural aspects of the pseudomorphs after garnet, discuss the mechanisms of garnet breakdown and the role of the liquid phase, and attempt to reconstruct the late pre-eruption metamorphic history of the sub-volcanic mantle.

This is a pre-copyedited, author-produced PDF of an article accepted for publication in Journal of Petrology *following peer review. The version of record* P. Špaček, L. Ackerman, G. Habler, R. Abart, and J. Ulrych: Garnet Breakdown, Symplectite Formation and Melting in Basanite-hosted Peridotite Xenoliths from Zinst (Bavaria, Bohemian Massif) J. Petrology (2013) 54 (8): 1691-1723 first published online May 31, 2013 doi:10.1093/petrology/egt028 *is available online at:* **http://petrology.oxfordjournals.org/content/54/8/1691**

2. GEOLOGICAL SETTING

The Bohemian Massif is a part of the European Variscides, representing a tectonic collage of continental terranes with contrasting tectonostratigraphic evolution. It is widely accepted that the orogen was formed by a diachronous accretion of several microcontinents, divided by domains with well developed oceanic crust and several active subduction zones between colliding Laurussia and Gondwana continents (e.g. Franke, 2000). As suggested by many authors, the orogenic process in the Bohemian Massif was largely controlled by a subduction of the Cambro-Ordovican oceanic lithosphere located between the Saxothuringian microcontinent and continental domains, which today are located to the southeast and south. The destruction of this ocean and following collision of the continental domains has left a suture located between the structurally lower Saxothuringian unit (SAX) to the northeast and north and structurally upper Teplá-Barrandian (TB) + Moldanubian (MOLD) units to the southeast and south (Fig. 1). The subduction seems to have operated since at least 400 Ma and is indicated by synchronous eclogitization of the Saxothuringian crust and its exhumation along the suture, the activity of a magmatic arc (Central Bohemian Plutonic Complex) and the tectonosedimentary evolution of the TB and MOLD units. The continental underthrusting of the Saxothuringian crust continued to ca. 340 Ma and lead to high-pressure metamorphism and imbrication of large parts of the Saxothuringian domain (e.g., Matte 1990; Franke, 2000; O'Brien 2000; Dörr & Zulauf, 2008; Schulmann et al., 2009 and references therein). Low- to medium-grade metamorphic rocks prevail in the SAX unit, while high-grade rocks are characteristic for the MOLD unit, nevertheless, both contain high-grade gneisses and felsic granulites with numerous bodies of spinel and garnet peridotites, often associated with eclogites. The garnet peridotites of asthenospheric and lithospheric heritage reveal a similar P-T record in both units (Medaris et al. 2006; Faryad et al. 2009; Schmädicke et al. 2010; Kotková et al., 2011) and suggest a large scale mixing of the high-grade domains during imbrication. Contrastingly, the TB unit, containing non-metamorphosed sediments of Lower Paleozoic age, represents a relatively subsided block between the other two units, their contact being marked by a steep zone of dip-slip mylonites and numerous syn-tectonic plutons (Dörr & Zulauf, 2008). During the Late Carboniferous the phase of Variscan compression was replaced by extensive wrench faulting and collapse of the orogen (e.g., Ziegler et al. 2006) associated with intense intrusive granitic magmatism and bimodal volcanism in Westphalian to Autunian (roughly 325 - 295 Ma; e.g., Siebel et al. 1997, Ulrych et al., 2006).

After a nearly 200 Ma long period of tectonic stability the Bohemain Massif was again partly mobilized in the late Cretaceous, as indicated by the formation of the transtensional Bohemian Cretaceous Basin in Cenomanian (Uličný, 2008) and by the development of the European Cenozoic Rift System (ECRIS; Prodehl et al., 1995) since the late Maastrichtian and Paleocene. The ECRIS is believed to have developed by passive rifting in the foreland of the Alps and the Pyrenees in response to the build-up of syn-collisional compressional intraplate stresses (Dèzes et al., 2004).

Magmatic activity in this system produced large volumes of volcanic rocks typically associated with subvolcanic complexes within rift-related grabens and in a broader region (e.g., Wilson & Downes, 2006; Lustrino & Wilson, 2007; Ulrych et al. 2011). This system of volcanic fields is often refered to as the Central European Volcanic Province (CEVP). A contribution of mantle plume to the magmatic activity was also suggested, based on seismic tomographic observations (Granet et al., 1995; Goes et al., 1999) and active rifting can not be ruled out.

The Cenozoic volcanism of the Bohemian Massif is of alkaline character. Tholeiitic basaltic rocks accompanying alkali basalts in other regions of the ECRIS, e.g. in the Vogelsberg Mts. and Hesse Graben, were not found in the Bohemian Massif. The age of the volcanics and subvolcanics ranges from late Upper Cretaceous to Quaternary, with several maxima of activity and its peak in the Late Oligocene and Early Miocene (22-32 Ma). While the early phases of magmatic activity are characterized by primitive, strongly Si-undersaturated subvolcanics of the melilite-nephelinite series, the differentiation of the primary magmas produced strongly alkaline (nephelinite–tephrite–

phonolite) and weakly alkaline (olivine nephelinite–basanite–trachyte) series in the period of peak activity (Ulrych et al., 2011).

The occurences of Cenozoic volcanic rocks in the Bohemian Massif form an arc-shaped belt which extends over 500 km from the western to the easternmost parts of the massif (Fig. 1). The more prominent western segment of the belt is associated with the SW–NE-trending, the >250 km long Eger Rift (Ohře Rift in Czech; here we prefer the more traditional name) stretching between the regionally important, steep, NW-SE striking Labe-Odra and Franconian fault systems, the latter representing the SW limit of the Bohemian Massif. The eastern segment of the volcanic belt contains mainly isolated volcanic complexes within the Labe–Odra fault system. The position of the Eger Rift largely coincides with the suture between SAX and TB+MOLD units, the rift graben covering most of its contact at surface. This strongly suggests a structural control of the Variscan suture on the Cenozoic volcanic activity (e.g. Kopecký, 1978; Babuška et al., 2009).

The sparse Pleistocene volcanics (2–0.26 Ma), extensive emanations of CO_2 and an unusual seismic activity indicate the local continuation of geodynamic processes, including deep magmatic activity, in the western part of the rift (Ulrych et al., 2011; Weinlich et al., 1999; Fischer and Horálek, 2003; Geissler at al., 2005) and, to a lesser extent, in the eastern part of the Labe-Odra Fault Zone (Špaček et al. 2010). Detailed seismological studies performed at local to regional scales in the western part of the rift indicate significant local updoming of MOHO to 27-26 km beneath the intersection of the Eger Rift with the Cheb-Domažlice Graben and regional updoming of the seismic low velocity zone to 90-65 km beneath the western Bohemian Massif (Babuška & Plomerová, 1992; Geissler at al., 2005; Heuer et al., 2006; Babuška et al., 2009).

The studied locality of Zinst is located at the SW-most margin of the rift, near the Franconian Fault, which bounds the crystalline basement of the Bohemian Massif against the Mesozoic cover sediments of the South German Block (Fig. 1). In this part of the rift sedimentary graben is not developed and the number and extent of Cenozoic volcanics is relatively small compared to the central and eastern parts of the rift. However, taking into account its position at the very contact of SAX and TB+MOLD units and the proximity of the domain to thinned seismic lithosphere, a complicated structure and evolution of mantle can be expected, including significant transformation during Cenozoic rifting and magmatic activity.

3. ANALYTICAL TECHNIQUES AND TERMINOLOGY

Major element compositions of minerals and fine grained aggregates were obtained on a Cameca SX100 electron microprobe at Masaryk University, Brno, using WDS. An accelerating voltage of 15 kV, a beam current of 20 nA and a beam diameter of 2 µm were used for most point analyses; for beam-sensitive phases (feldspars, carbonates, apatite) reduced current (10nA) and larger beam (5µm) were used. Integrated compositions of fine grained mineral aggregates were analysed by scanning the beam over areas of 20×15 or 50×38 µm. Counting times were 10s for major elements and 20-60s for minor elements. Alkalis were counted early in the analysis to reduce the effect of their migration. Natural and synthetic minerals were used as calibration standards and all data were reduced using the PAP correction routine (Pouchou & Pichoir, 1991).

The spatial distribution of feldspar and carbonate in symplectites was studied in an optical microscope equipped with a hot cathode (HC2-LM, Simon Neuser) at Masaryk University, Brno.

Whole-rock major element concentrations in the host basanite were determined at Charles University, Prague, using wet chemical methods. Analyses of the reference standard and duplicate analyses of the samples yield total errors of ±5 % (1σ).

Trace element concentrations in symplectites and clinopyroxenes were determined in polished, >100 µm thick sections at the Institute of Geology, ASCR, Prague, using a Thermo-Finnigan Element 2

sector field ICP-MS coupled with 213 nm NdYAG laser. The sample introduction system was modified to enable simultaneous nebulization of a tracer solution in Ar and laser ablation particles in high purity He of the solid sample (Horn et al., 2000). This setup allows appropriate tuning of the instrument and monitoring of ICP-MS stability during laser ablation, aspirating natural ^{205}Tl as the tracer solution through an Aridus II^{TM} desolvating nebulizer (CETAC Technologies). A laser beam with a pulse frequency of 20 Hz and energy of ~7 J/cm^2 was used. Element concentrations were analysed in 80×100 µm domains. All data were calibrated against the external standard of synthetic silicate glass NIST SRM 612. ^{44}Ca was used as internal standard for signal fluctuation. Time-resolved signal data were processed using the Glitter software (GEMOC, ANU). Values from Pearce et al. (1997) were used for calculation of the corresponding element concentration.

EBSD analyses were performed on a FEI^{TM} Quanta 3D FEG instrument at the Department of Lithospheric Research (University of Vienna, Austria). The system is equipped with a field-emission electron source and an EDAX^{TM} Digiview IV EBSD camera. The OIM^{TM} Data Collection and Analysis software packages were used for data acquisition and processing. Samples were prepared as polished thin sections applying mechanical and final chemo-mechanical polishing. For final preparation a colloidal silica suspension with pH 9.2-10 was used as polishing agent on a rotary polisher. Conducivity of the sample surface was established by very thin carbon coating using a single carbon thread at vacuum conditions of <10^{-5} mbar during evaporation. EBSD-analyses were performed at a working distance of 10 mm and 70° sample tilt. Beam settings were at 15kV accelerating voltage and 4 nA beam current in analytic mode (SEM aperture 1 mm). A 2x2 binning of the EBSD camera-resolution has been applied for phase identification, whereas a 4x4 binning has been used for EBSD mapping. Hough settings of 1° theta step size, a binned pattern size of 160 pixels, a 9x9 convolution mask and a minimum peak distance of 10 degrees were applied for indexing 6 - 12 Hough peaks. EBSD mapping has been performed using beam scanning at step sizes of 0.15-0.4 micrometers. Data were processed using the „Grain CI standardization" cleaning routine of the OIM^{TM} DC software, which unifies the confidence index of adjacent datapoints without changing any crystallographic orientation. Subsequently, datapoints with CI < 0.1 were discarded.

Modal compositions were calculated from BSE images or computer-processed, manually digitized optical scans of thin sections in plane-polarized and cross polarized light. Mineral abbreviations are as follows: Ab-albite, Afs-alkali feldspar, Alm-almandine, An-anorthite, Apa-apatite, Cpx-clinopyroxene, Crb-carbonate, Fo-forsterite, Gei-geikielite, Grs-grossularite, Grt-garnet, Mgts - Mg-Tschermak's molecule, Ol-olivine, Opx-orthopyroxene, Or-orthoclase, Pl-plagioclase, Prp-pyrope, Rut-rutile, Spl-spinel, Sps-spessartite, Tfs-ternary feldspar. Cation concentrations are given in atoms per formula unit (a.p.f.u.) or in atomic ratios, where Mg# = 100 × Mg / (Mg + Fe), and Cr# = 100 × Cr / (Cr + Al).

The usage of the terms *symplectite* and *kelyphite* is often confusing in descriptions of reaction coronae. In this text the term *symplectite* is used for any intimate intergrowths of two or more mineral phases with systematic crystallographic relations, while the term *kelyphite* emphasizes the shell-like morphology of the reaction corona or its particular zone. The term *pseudomorph* is used with a more general meaning to denote the mineral aggregates related to former garnet.

4. ZINST BASANITE AND XENOLITH SUITE

The eroded relic of volcanic breccia and lava flow near Zinst is exposed in an active quarry located at 49.901°N, 11.943°E, in the SW-most part of the Eger Rift, <1km to the NE from the trace of the Franconian Fault (Fig.1). The age of the lava was dated at 28.8 Ma (Todt and Lippolt, 1975) or 25.6 Ma (Horn and Rohrmüller, 2005) which is in the Late Oligocene to Early Miocene range characteristic for volcanic bodies of the basanite–olivine nephelinite series in the SW part of the rift. The chemical

composition of the lava corresponds to nepheline basanite with phenocrysts of Ol > Cpx (about 20 vol%) in matrix formed by Cpx > Pl > Ne/Afs > magnetite ± olivine, apatite, analcime and zeolites. By its alkaline composition, high Na_2O/K_2O ratio and enrichment in incompatible elements and LREE (Table 7, Electronic appendix 1), the Zinst basanite is close to the main basaltic rock types occurring in the whole Eger Rift. Similarly, the initial $^{87}Sr/^{86}Sr$ (0.7035) and $^{143}Nd/^{144}Nd$ (0.51259) ratios are within the range of the mafic Cenozoic volcanics in the Bohemian Massif (recent, unpublished data and Ulrych et al., 2011).

The exposed parts of Zinst basanite contain unusually abundant spinel peridotite xenoliths, with mostly rounded spherical to ellipsoidal shape and typical diameters of 3-10 cm (occasionally up to 30 cm). The xenolith suite was described briefly by Huckenholz & Kunzmann (1993). Lherzolites with Ol>>Opx>Cpx>>Spl strongly prevail in the suite over less common harzburgites. The distribution of clinopyroxene is often irregular within the xenolith, and exceptionally small-scale domains enriched in Cpx were observed corresponding to olivine websterite/pyroxenite. Granular textures with 0.5-4 mm large, strain-free, equant grains predominate. High aspect-ratio tabular grains of olivine with plane-parallel faces are often observed in the coarser types. Nevertheless, the textures are only rarely well equilibrated and olivine typically displays non-unimodal grain size distribution and variable grain shape with curvilinear boundaries. Rare transitions to porphyroclastic textures in some xenoliths suggest weak, late high-stress deformation. The grain size of pyroxenes is similar to that of olivine and their grain shape is typically convex, displaying no indication of late crystallization relative to olivine. The content of spinel is generally low, and its habit is largely variable, ranging from irregular to perfectly rounded shapes. In some samples larger clusters of coarse grained Opx+Cpx+Spl are present in the rock. Neither amphibole nor phlogopite were found in Zinst peridotites. In this respect the Zinst xenolith suite is similar to xenolith suites described from most other parts of the Bohemian Massif (Fediuk & Fediuková, 1989; Medaris et al., 1997; Ackerman et al. 2007; Matusiak-Małek et al. 2010), where metasomatic hydration of the sub-volcanic upper mantle is only rarely observed (Kramer & Seifert, 2000; Geissler et al., 2007).

Although a fresh primary mineral assemblage is well preserved in most xenoliths, grain boundary veinlets are often observed, together with extensive cracks, and arrays of fluid inclusions in healed cracks in all mineral phases. In some xenoliths pyroxenes (mainly Opx) are partly or completely altered due to the reaction with grain boundary melts. Xenoliths with larger silicate and/or carbonate melt pockets are relatively abundant, too. In several samples late chlorite and zeolites were observed, filling small pores. Up to 2 mm thick rims of calcitic carbonate are developed around some xenoliths, often accompanied by local, vein-like carbonate accumulations in adjacent parts of host basanite.

A unique feature of the Zinst xenolith suite is the presence of xenoliths with sub-centimetre sized, pseudo-spherical clusters of pyroxenes, spinel and plagioclase. As described below, the content of fine grained symplectites with specific chemical composition in the cores of these clusters suggests that they were formed from a garnet presursor, hence these clusters are henceforth referred to as „garnet pseudomorphs“. Xenoliths with pseudomorphs after garnet are very rare in the Zinst lavas, with an estimated abundance <2% of the xenolith suite. Similar features have not been described earlier from other localities of Cenozoic volcanics in the Bohemian Massif and Central Europe, from where only mantle peridotites and pyroxenites which were completely equilibrated in the spinel stability field have been reported so far.

5. PSEUDOMORPHS AFTER GARNET

The minerals pseudomorphing garnet form 0.5-10 mm large, mostly oval or spheroidal clusters composed of one to four microstructurally and chemically distinct concentric zones (Figs. 2-4) which can be correlated from sample to sample throughout the xenolith suite:

This is a pre-copyedited, author-produced PDF of an article accepted for publication in Journal of Petrology *following peer review. The version of record* P. Špaček, L. Ackerman, G. Habler, R. Abart, and J. Ulrych: Garnet Breakdown, Symplectite Formation and Melting in Basanite-hosted Peridotite Xenoliths from Zinst (Bavaria, Bohemian Massif) J. Petrology (2013) 54 (8): 1691-1723 first published online May 31, 2013 doi:10.1093/petrology/egt028 *is available online at:* **http://petrology.oxfordjournals.org/content/54/8/1691**

Zone I (rim) with aggregates of millimetre-sized orthopyroxene + clinopyroxene ± olivine grains with granular texture and sub-millimetre interstitial grains of brown spinel,

Zone II with mosaic intergrowths of orthopyroxene (grain size in the order of 100 μm) and sub-idiomorphic light pink spinel (order of 10 μm),

Zone III with generally radially fibrous intergrowths of orthopyroxene (grain size in the order of 10-100 μm) and light-pink spinel (order of 10 μm), usually containing interstitial plagioclase, and

Zone IV (core) consisting of intimately intergrown submicron-sized grains of orthopyroxene, spinel and anorthite. The ultra-fine grain size of phases in this zone causes quasi-opaque appearance and dark red-brown coloring in plane polarized light.

Disregarding the specific features of each zone, there is a major microstructural difference between the granular and coarse grained Zone I, where pyroxenes have similar microstructure as in the host peridotites, and the finer grained Zones II-IV, which are symplectites with smaller grains of spinel enclosed in larger orthopyroxene crystals (Figs. 3 and 4).

Based on the presence of individual symplectite zones, four basic types of pseudomorphs after garnet are distinguished (Figs. 2 and 4): Type A with Zones III+IV and minor domains of Zone II, Type B with Zones II+III, Type C with Zone III only and Type D with Zone II only. The occurrence of Zone I around symplectites is variable and does not correlate with the internal microstructure of the symplectite domains. In most samples, only Zones I-III are developed, whereas the complete, four-zone sequence is rarely observed. Boundaries between Zones I/II, I/III, III/IV are sharp, while those between Zones II/III are often gradual. An important, inherent feature of Type A pseudomorphs are silicate veinlets spreading radially from the symplectite, typically terminated at the interface between Zones III and IV (Figs. 2, 13 and 14d).

In addition to the generally concentric arrangement of the zones outlined above, smaller domains of Zone III symplectites are also observed in the interior of Zone IV (Figs. 4a, b) which itself has a domain sub-structure (Fig. 6).

Although the precursor garnet was never observed in the samples studied, its former presence is inferred from the local bulk major and trace element composition of the ultrafine grained Zone IV. In most samples, the outer parts of the symplectite are strongly Na-metasomatised and contain abundant plagioclase-rich or carbonate-rich melt pockets and related products of retrograde reactions. Mineral chemistry and bulk compositions of individual zones and metasomatised domains are described below, together with more details on their microstructures. The xenoliths with Type A pseudomorphs are extremely rare (<0.1% of xenolith suite) and, despite large effort, only three samples have been found up to now. The description given below is based upon 9 representative samples with Type B, C and D pseudomorphs and 2 samples with Type A pseudomorphs.

5. MICROSTRUCTURE AND MINERAL CHEMISTRY

5.1. HOST PERIDOTITE AND ZONE I

Peridotites hosting pseudomorphs after garnet exhibit similar microstructures and modal compositions as the pseudomorph-free types, decribed briefly in Section 4. Content of spinel seems to be higher in samples with pseudomorphs. The outer part of the pseudomorphs, Zone I, is represented by clusters of clinopyroxene + orthopyroxene + spinel grains forming up to several millimetre thick rims. The extents and modal compositions of these clusters are variable. In some samples both pseudomorphs with and without Zone I are observed, in other samples Zone I is entirely missing. On the contrary, one sample contained abundant small symplectites within several-centimetre wide, pyroxene-rich, spinel-free domains, corresponding to olivine websterite or

pyroxenite. In many thin sections similar clusters without symplectite cores are observed, likely representing the external parts of symplectite-bearing patches centered out of the section. The microstructure in Zone I is very close to that in the host peridotites and the modal proportions of the mineral phases is the main difference between the two. Olivine is only a subsidiary phase in well developed Zone I. The modal proportions analysed in seven well-defined clusters show large variations in the range Opx_{28-64} Cpx_{30-67} Spl_{5-12} (rare olivine grains were excluded from counting).

Clinopyroxene grains often exhibit crescent shapes when in contact with symplectite, sometimes forming narrow local rims of the latter (Fig. 5a). In contrast, olivine grains are often convex, prograding into symplectite. Orthopyroxene grains display both types of habit, although the wide-crescent shape prevails. Spinel grains, usually around 200 μm, exceptionally up to 800 μm large (longest dimension), typically occur in intergranular positions and usually are associated with orthopyroxene or clinopyroxene. Spinel grains display variable shapes from sub-idiomorphic, to concave polygonal and often make atoll-like embayments or complete rims around other phases, typically around small clinopyroxene grains (Fig. 5a). Inclusions of spinel in orthopyroxene are rare.

The mineral compositions of the phases in Zone I and in the host peridotites are very close to each other (Tables 1-4). Olivine, orthopyroxene and clinopyroxene are magnesian, with Mg#s 89.4-90.7, 90.3-91.1 and 89.3-91.1, respectively. The NiO content in olivine ranges from 0.29 to 0.48 wt%. Pyroxenes are homogeneous and free of exsolution lamellae. Orthopyroxene has low contents of Al (0.18-0.22 a.p.f.u.), and Ca (0.032-0.037 a.p.f.u.). Clinopyroxene has a relatively narrow range of Cr# (7.4-11.7) and Na-contents (0.08-0.13 a.p.f.u.) and is Ca-poor (0.735-0.783 a p.f.u.). The compositional range of spinel is comparatively large (Mg# = 72.0-77.7; Cr# = 13.1-24.9).

In general, the range of Mg# and Ca-, Al-, Cr-, Ni-, Mn-contents in olivine, pyroxenes and spinel of host rock and Zone I largely overlap (Figs. 7-11). Zone I displays slightly but systematically higher Al-contents and lower Ni-contents in orthopyroxene and lower Cr# in clinopyroxene. Typically, slightly lower Cr# and Mg# of spinel are observed in Zone I as compared to the host peridotite.

5.2. ZONE II

Zone II is often developed around fibrous Zone III, usually as <300 μm thick rims in Type B pseudomorphs. In many samples, however, it is only locally developed or entirely missing (Type C pseudomorphs), limited either to narrow rims or laterally isolated patches. Exceptionally, this zone forms entire symplectites up to >2 mm large (Type D pseudomorphs). In some cases the transition between the Zones II and III is rather gradual which makes their distinction difficult. In other samples, on the other hand, the boundary between Zones II and III is sharp and hence both zones are treated independently.

In thin-section, this zone is characterised by isolated sub-idiomorphic, small (50-100 μm), low aspect ratio grains of light-pink spinel enclosed in larger (order of 100 μm) crystals of orthopyroxene. In Type D, only a few orthopyroxene grains constitute the entire symplectite. The spatial organization of spinel grains in orthopyroxene is regular so that the symplectites have a mosaic-like structure (Figs. 4e and 14b). The orthopyroxene of Zone II usually shows topotactic relations to the adjacent orthopyroxene in Zone I or in the host peridotite.

Clinopyroxene is rare as primary phase in Zone II. Abundant larger, irregularly shaped grains of clinopyroxene were observed in the outer part of the symplectite or at its boundary with Zone I in one unique sample only.

In addition to the above described symplectite assemblage, Zone II always contains substantial amounts of secondary, plagioclase-rich melt pockets or carbonate pockets (see Chapter 6.5). Taking

This is a pre-copyedited, author-produced PDF of an article accepted for publication in Journal of Petrology *following peer review. The version of record* P. Špaček, L. Ackerman, G. Habler, R. Abart, and J. Ulrych: Garnet Breakdown, Symplectite Formation and Melting in Basanite-hosted Peridotite Xenoliths from Zinst (Bavaria, Bohemian Massif) J. Petrology (2013) 54 (8): 1691-1723 first published online May 31, 2013 doi:10.1093/petrology/egt028 *is available online at:* **http://petrology.oxfordjournals.org/content/54/8/1691**

into account their significant volume, we cannot rule out that these features are actually pseudomorphs after some other phase, e.g. clinopyroxene, present in the symplectite prior to melting. For this reason the primary mineralogical composition of Zone II is uncertain.

The compositions of orthopyroxene and spinel in the Zone II differ significantly from the respective phases in the host peridotite and in Zone I (Tables 1 and 3, Figs. 7, 8 and 10). In Zone II orthopyroxene has lower Mg# (86.9-89.6) and higher Ca content (0.050-0.077 a.p.f.u.). Spinel has lower Cr# (5.6-10.5). The Mn-content in orthopyroxene is higher by a factor of 3 and the Ni-content in both orthopyroxene and spinel is lower by nearly one order of mangitude than in the respective phases of the Zone I. On the other hand, mineral compositions of orthopyroxene and spinel in Zone II are very close to those in Zone III in most aspects. Only the Cr- and Al-contents in orthopyroxene seem to exhibit gradual increase from Zone I towards Zone III in some samples. However, this could partly be the effect of larger heterogeneity of content of these elements in orthopyroxene of the two zones.

5.3. ZONE III

Zone III is by far the most abundant feature in the symplectites, typically forming 250-700 µm wide kelyphitic rims around Zone IV in Type A pseudomorphs, or 0.5-7 mm large, rounded cores of Type B and C pseudomorphs. Within Zone IV smaller patches of Zone III symplectite are present, forming promontories, spheroidal islets partly arranged along trails, or elongated domains supposedly developed along former cracks (Fig. 4a, b). The interface between Zone III and ultra fine grained symplectite of Zone IV is always sharp, with straight or gently curved traces of the boundary segments (Figs. 4b and 5c, h).

The internal microstructure of this zone is generally radially fibrous, typically defined by fan-shaped aggregates of elongated grains of orthopyroxene and spinel. In Type A pseudomorphs the grain long axes are mostly perpendicular to the interface between Zone III/Zone IV, but often clearly deflected from this direction (Fig. 5h). However, at small scale the grain orientation is highly variable, probably partly depending on the position of these zones relative to the section plane. In some samples, significant lowering of the grain aspect ratio and slight coarsening in an outward direction is observed, locally leading to gradual transition to Zone II.

The characteristic apparent grain size is in order of 100 µm for orthopyroxene and in order of 1-10 µm for spinel. In the non-fibrous parts of Opx+Spl intergrowths, up to 400 µm large Opx single-crystals form a continuous matrix. In domains of radial Opx fibers apparently isolated, typically 5-20 µm wide and 50-100 µm long orthopyroxene laths are developed. Spinel grain sections in the same domain are generally smaller, mostly enclosed in orthopyroxene, and less frequently located in interstitial positions associated with plagioclase. Spinel displays variable habit in thin-sections: larger convex or concave polygonal grains with lower aspect ratio, grains with partly developed crystal faces, often as parallel V-shaped twins resembling graphic or feather texture. Simple, long and narrow straight lamellae are also developed, mainly in the anorthite-rich parts of the zone. In addition to this, low aspect ratio, more rounded, single grains are developed in contact with anorthite. EBSD mapping indicates that the grain sections of spinel enclosed in orthopyroxene typically belong to larger grains with complex 3D morphology (Fig. 5e). The topotactic relations between Opx and Spl correspond to those described by Obata & Ozawa (2011). Opx (100) is parallel to one of the four equivalent Spl (111) planes, whereas Opx (010) is parallel to one of the six equivalent Spl (110) planes (Habler et al., in preparation).

Anorthite is located in interstitial positions, having variable morphology from several-µm-thick films at Opx and Spl phase boundaries to tens of µm large pools. In Type A pseudomorphs clear

segregation of anorthite into larger interconnected pools separated by orthopyroxene laths is observed near and at the interface with Zone IV, while it is often entirely missing in the less clearly "fibrous" Opx+Spl aggregate in domains more distant from the interface (Figs. 5c, f, h). EBSD mapping revealed that these interstitial anorthite domains are polycrystalline aggregates of 0.5-5 µm large grains (Fig. 5f), i.e. approximately one order of magnitude smaller than the width of the Opx laths. In many samples small (0.2-2 µm), bubble-shaped pores are observed in varying amounts within the anorthite domains (Fig. 5i).

Clinopyroxene is rare in Zone III and, similar to Zone II, mostly associated with feldspar-rich pockets interpreted as crystallized melt (see Chapter 6.5). Exceptionally, small, irregularly shaped clinopyroxene grains are observed in the symplectite, without any feldspar present. These seem to represent a part of the primary mineral assemblage which is not related to later melt formation.

The modal proportions of the constituent minerals of Zone III are relatively homogeneous: mineral modes of $Opx_{57-64}Spl_{23-31}Pl_{10-15}$ were measured in local domains in Type B pseudomorphs and $Opx_{64}Spl_{23}Pl_{13}$ with sporadic Cpx grains (< 0.1%) in an apparently isolated domain within Zone IV of a Type A pseudomorph.

The bulk composition of pristine inner parts was measured in several samples by electron microprobe scanning the electron beam over an area of 20×15 µm or 50×38 µm. On average the composition is very similar to that of Zone IV (Table 6). The variations in Si-, Mg- and Ca-contents seem to correlate with the modal abundance of An which is heterogeneously distributed.

Spinel and plagioclase seem to be compositionally homogeneous at grain scale. In spite of substantial variations at the sample scale, spinel has higher Al- (Cr# = 5.5-9.5) and lower Ni-content than in the host peridotite and in Zone I, but is similar to spinel in Zone II. The composition of plagioclase is close to anorthite ($An_{92.5-96.5}Ab_{3.5-7.3}Or_{0.04-0.17}$) in the pristine inner parts of Zone III (Table 5, Fig. 12).

Orthopyroxene is similar to that in Zone II, showing higher Fe- (Mg#=85.4-88.2), Ca- (0.047-0.085 a.p.f.u.), and Mn-contents than in the host peridotite and in Zone I. However, in terms of Al- and Cr-contents, orthopyroxene displays significant compositional variability. EDS-element mapping partly combined with EBSD-mapping in the chemically pristine „islet" domains of Zone III within Zone IV show intragranular acentric chemical variations indicating the presence of two types of orthopyroxene with different Al-contents: a high-Al orthopyroxene with 28-35 mol% of Mgts and a low-Al orthopyroxene, similar to that in Zone II, with 13-14 mol% Mgts (Figs. 5g and 8; Table 1).

Clinopyroxene exhibits low Mg# (84.1-85.9) and Na-content (<0.015 a.p.f.u.), and a relatively wide range of Ca-content (0.587-0.832 a.p.f.u.) and Cr# (2.3-9.0) (Table 2, Fig. 9).

Single-crystal inclusions of rounded olivine and clinopyroxene grains and sub-idiomorphic spinel grains were observed within symplectites in several samples (Zones III and IV, see Fig. 9-11 for mineral compositions and Electronic Appendix 2 for photographs). No significant reaction coronae or chemical zonations are developed around these grains. Olivine inclusions usually display a rimward increase in Fe content.

5.4. ZONE IV

Zone IV is composed of a very fine grained aggregate of intimately intergrown orthopyroxene, spinel and plagioclase as identified by EBSD analysis. The mineral aggregates are organized into domains with internally constant or gradually varying shape preferred orientation, often abruptly changing at subdomain boundaries (Fig. 6a). Two microstructurally different types (IVa, b) are discerned within the chemically pristine parts of the zone. Locally, late metasomatism lead to additional structural

This is a pre-copyedited, author-produced PDF of an article accepted for publication in Journal of Petrology *following peer review. The version of record* P. Špaček, L. Ackerman, G. Habler, R. Abart, and J. Ulrych: Garnet Breakdown, Symplectite Formation and Melting in Basanite-hosted Peridotite Xenoliths from Zinst (Bavaria, Bohemian Massif) J. Petrology (2013) 54 (8): 1691-1723 first published online May 31, 2013 doi:10.1093/petrology/egt028 *is available online at:* **http://petrology.oxfordjournals.org/content/54/8/1691**

transformation which is described separately in the following chapter. In domains IVa and IVb, similar topotactic relations between Opx and Spl occur as described with Zone III and reported by Obata & Ozawa (2011). Opx (100) coincides with one Spl (111) and Opx (010) coincides with one Spl (110) plane.

Type IVa is represented by an about 10-30 µm wide, semicontinuous band preferentialy developed along the Zone III/Zone IV interface (Fig. 6a). The mineral grains are strongly elongated in the direction (sub)perpendicular to this interface. The band of type IVa symplectite retains relatively constant width and mimics the shape of the Zone III/Zone IV interface in every detail, suggesting growth at a constant rate and postdating the formation of the Zone III. The symplectite matrix is comprised of orthopyroxene and plagioclase, which alternate at nearly regular intervals of 200 to 500 nanometers. Spinel occurs as extremely fine, tens of nm wide lamellae or rods always enclosed in Opx (Fig. 6b). The microfabric is constant within the band and no grain coarsening towards its margins is observed.

Type IVb symplectite (Fig. 6b) constitutes the major part of Zone IV and forms isometric, 30-150 µm large microstructural subdomains. These domains are constituted by the same mineral assemblage as Type IVa. The main difference is the lower aspect ratio of individual mineral grains in Zone IVb. In particular, spinel forms nearly isometric grains enclosed within Opx or along the Opx-Pl phase boundaries. Both the Opx and the Pl still show some grain elongation, and their shape preferred orientation is continuous across the boundary between type IVa and type IVb symplectite, whereas it may gradually change farther from the boundary.

The bulk chemical composition of the pristine parts of Zone IV measured by EMPA in scanning mode (areas 20×15 µm) corresponds to the composition of pyrope-rich garnet $Prp_{71.1\text{-}72.2}Alm_{14.2\text{-}15.2}Grs_{12.3\text{-}13.9}Sps_{0.7\text{-}0.8}$ and is within the range of compositions of alpine-type peridotite garnets from the Bohemian Massif. Locally, possible minor enrichment in Na is indicated by increased concentrations (0.17-0.37 wt% Na_2O). The compositions of the symplectite-forming mineral phases could not be analysed due to their small grain size.

In sample ZIN2A, an isolated, barrel-shaped inclusion of Fe-rich olivine was observed within Zone IV, with similar composition to the above described inclusions in Zone III (Electronic Appendix 2). The olivine grain displays chemical zoning with a more magnesian core (Mg# = 87.0-85.8), but no significant reaction corona is developed at its grain surface, except for minor, late Na-metasomatism in the adjacent symplectite.

5.5. LATE METASOMATIC AND MELT-RELATED FEATURES

In addition to the primary mineral assemblages described above, most xenoliths from Zinst contain finely crystallized material from melts/fluids of external origin. The outer parts of the symplectites are usually strongly affected by metasomatic fluids and/or melts as indicated by high content of melt pockets, Na-enrichment of plagioclase and, locally, total obliteration of primary mineralogy and texture. Furthermore, intense, localized melt transfer occured during the late stages of xenolith evolution via radial silicate veinlets associated with Type A pseudomorphs. A more pervasive percolation of similar agents is indicated by thin (<30 µm) intergranular veinlets with dominant alkali feldspar and clinopyroxene or carbonate commonly observed along grain contacts in the host peridotite and in Zone I. The most important metasomatic features are described in following paragraphs and illustrated in Fig. 13. Selected representative major element mineral compositions are given in Tables 2, 4-5 and Electronic Appendices 1 and 3.

Outer rims of symplectite

This is a pre-copyedited, author-produced PDF of an article accepted for publication in Journal of Petrology *following peer review. The version of record* P. Špaček, L. Ackerman, G. Habler, R. Abart, and J. Ulrych: Garnet Breakdown, Symplectite Formation and Melting in Basanite-hosted Peridotite Xenoliths from Zinst (Bavaria, Bohemian Massif) J. Petrology (2013) 54 (8): 1691-1723 first published online May 31, 2013 doi:10.1093/petrology/egt028 *is available online at:* **http://petrology.oxfordjournals.org/content/54/8/1691**

Irregular zones characterized by substantial content of finely crystallized silicate or carbonate melt are developed in the outer parts of most symplectites. The width of this „aureole" is largely variable: in Type B-D pseudomorphs the melt typically projects from larger pockets deep into the symplectite (e.g., Fig. 14a) forming thin films of alkali-rich plagioclase at most Opx-Spl phase boundaries, while in Type A pseudomorphs only a 100-400 μm wide outer rim is affected by metasomatism. Three types of metasomatic domains are distinguished in symplectites based on the degree of overprint and progress of retrograde reactions:

SM domains (sodic metasomatism) are defined by similar texture and modal mineralogy as the pristine symplectite described above, with plagioclase significantly more sodic than in the pristine parts of the symplectite (Fig. 12). In contrast to the radial veinlets and OP domains described below, the potassium content in the feldspars is only slightly increased relatively to the pristine symplectite. Despite the textural similarity, the boundary between SM domains and the pristine symplectite is typically sharp as revealed by element mapping.

MM domains (metasomatic melting) are defined by the abundance of finely crystallized melt in variably shaped pockets. Orthopyroxene adjacent to melt pockets usually displays corrosive morphologies with embayments, indicating partial resorption. Spinel grains have small aspect-ratios and usually display chemical zoning when in contact with melt pocket. Locally, Fe-Ni-Cu sulphides, Fe-rich spinel and rutile are present.

Silicate and carbonate pockets are distinguished in the MM domains, where the latter typically form inclusions in the former, indicating that both types are genetically related to each other. The silicate pockets are variably shaped, usually with small aspect ratio, and often linked by plagioclase-rich films at grain boundaries of coarser orthopyroxene and spinel grains. The mineral composition is strongly variable, dominated by plagioclase hosting numerous small, rounded inclusions of clinopyroxene or olivine. Typically, plagioclase has andesine composition with less than 4% orthoclase content (Fig. 12). In Zone II, larger relict grains of clinopyroxene with complicated embayments at the contacts to the pockets are locally observed, suggesting partial resorption. The bulk compositions of pockets (free of larger phenocrysts) correspond to Ab+An±Ne±Di±Hy±Ol-normative basalt to basaltic andesite with very low K-contents (0.07-0.49 wt% K_2O; Electronic Appendix 1). In some samples, spherical vesicles filled with secondary hydrated silicates were observed in larger pockets (Fig. 14b).

The carbonate pockets usually occur as variably shaped, rounded inclusions within the silicate melt pockets, and a clear genetic link between the two types is apparent (Fig. 14e). In most cases the carbonate pockets are formed only by carbonate or by the association Crb+Ol. In more intensely molten symplectites, complex mineral assemblages were observed: Crb+Ol+Apa+Gei+Cpx+Rut+loveringite. The minerals enclosed in carbonate pockets exhibit euhedral faces at contacts with carbonate. Olivine has a wide range of Mg# and Ni contents and clinopyroxene is rich in sodium (Figs. 9 and 11). A high temperature origin of this type of carbonate pocket is indicated by the large Mg-content in carbonate containing up to 44 mol% magnesite component (Electronic appendix 3). The grain-size of carbonate is extremely small, below the resolution of the optical microscope.

OP domains (olivine-plagioclase) are locally developed within MM domains and are defined by small-scale vermicular intergrowths of olivine and plagioclase growing at the expense of orthopyroxene. These domains are commonly observed in the proximity of the radial veinlets where the Ol+Pl intergrowths completely overprint the original structure (Fig. 14f). They are typically accompanied by variable increase of the potassium content in feldspar relatively to the pristine parts of symplectite.

Radial silicate veinlets

This is a pre-copyedited, author-produced PDF of an article accepted for publication in Journal of Petrology *following peer review. The version of record* P. Špaček, L. Ackerman, G. Habler, R. Abart, and J. Ulrych: Garnet Breakdown, Symplectite Formation and Melting in Basanite-hosted Peridotite Xenoliths from Zinst (Bavaria, Bohemian Massif) J. Petrology (2013) 54 (8): 1691-1723 first published online May 31, 2013 doi:10.1093/petrology/egt028 *is available online at:* **http://petrology.oxfordjournals.org/content/54/8/1691**

Up to several cm long, 100-300 µm wide, transgranular veinlets are observed in radial arrangement around symplectites of the Type A pseudomorphs (Figs. 2 and 14d). The coincidence with Type A pseudomorphs is invariable; such veinlets are never observed in other pseudomorphs. The veinlets usually appear to be blind in thin sections (Figs. 13, 14c), only some continue to the margin of the xenolith. They are typically sharply terminated at the Zone III/IV boundary, thinning farther away from the symplectite and branching into several intergranular veinlets at the outer end. The mineral assemblage of the vein fill is dominated by plagioclase + ternary feldspar (Fig. 12) and associated Oli+Cpx+Gei+Apa+Spl+Ilm+Rut.

Close to the symplectites, reaction rims are developed in orthopyroxene grains at the contact with the veinlets. The reaction rims generally show a sequence of layers comprising: host Opx — Al-poor rim (same grain) — Al-poor Cpx+Ol+Afs — Ol+Afs — veinlet. The rims of olivine and clinopyroxene of the host peridotite and Zone I in contact with the silicate veinlets are enriched in Fe and Ca. In some veinlets it is clearly observed that the width of the melt-Opx reaction zone decreases with increasing distance from the symplectite. In the outermost parts of the veinlets, the modal reaction between Opx and melt may be entirely missing (Fig. 13).

6. TRACE-ELEMENT CHEMISTRY OF THE SYMPLECTITES

The major element bulk compositions of the symplectites given above indicate a chemical affinity between the inner Zone IV and the fibrous Zone III, suggesting that both were originally produced by isochemical breakdown of garnet. In contrast, the modal compositions and textures in the outer parts of the symplectites (domains SM and MM in Zones II and III) indicate strong metasomatism by Na-rich melts with decreasing intensity of the metasomatic overprint from rims to cores. In order to discuss this phenomenon in more detail, trace element concentrations were measured by LA-ICP-MS (Table 7) along core-to-rim profiles across symplectites in three samples representing Type A pseudomorphs (ZIN2 and ZIN50) and Type C or B/C pseudomorphs (ZIN53). A beam size of 80 µm was used to analyse local bulk compositions in the fine grained mineral aggregates. Chondrite-normalized (Boynton, 1984), rare earth element (REE) patterns and primitive upper mantle-normalized (PUM; McDonough and Sun, 1995) trace element patterns are given in Fig. 15 for all analyzed zones as well as for host basanite and clinopyroxene.

Zone IV displays similar trace element compositions in both symplectites of Type A (samples ZIN2 and ZIN50). The LREE-depleted and HREE-enriched patterns (La_N/Yb_N = 0.001-0.006) and the significant depletion in most trace elements (e.g., large ion lithophile elements - LILE, Th, U) are compatible with the compositions of typical peridotitic garnets. No systematic compositional variations were observed between cores and rims of this zone. In the pristine, inner parts of Zone III (sample ZIN2), the trace element compositions generally range within those observed in Zone IV, and they are nearly identical to each other within the same pseudomorph. The high variations in Ba-content in Zone IV (<0.045 to 0.98 ppm) are probably due to late metasomatic alterations along fractures, as indicated by small baryte grains locally observed in the altered parts of this zone. Similar enrichment was only rarely observed in the analysed pristine domains of Zone III, however, some parts of this zone are locally enriched in Sr.

Contrastingly, the metasomatised or melt-pocket bearing, outer parts of the symplectites of the A-Type pseudomorphs (ZIN2, ZIN50) show different degrees of enrichment in LREE (La_N/Yb_N = 0.007-0.111), LILE and some other trace elements (e.g., Li, U) coupled with depletion in Zr, Hf and MREE, both usually increasing towards the rims. In sample ZIN50, for example, concentrations increase from 0.01 to 0.5 ppm for La, 0.04 to 3.3 ppm for Rb and 0.3 to 31 ppm for Li between Zone IV and outer MM/OP domains. The Pb contents sometimes yield very high values (up to 2.8 ppm) similar to those

in host basanite (2.6 ppm). Similar compositional patterns were observed in Type C or B/C pseudomorphs (ZIN53) with differences between cores and rims being less expressive.

7. GEOTHERMOMETRY

As indicated by symplectites with habits and bulk compositions corresponding to garnet, we can assume that these samples represent former five-phase peridotites (Ol+Opx+Cpx+Spl+Grt) with relatively large garnet grains present prior to its breakdown to symplectite. The formation of Zone I documents the passage of the samples from the garnet to the spinel stability field and suggests that garnet was metastable. For this reason barometers calibrated for garnet peridotites could not be applied.

Similar mineral compositions and textures indicate that the host peridotite and Zone I equilibrated under the same pressure-temperature conditions. Temperatures of equilibration were calculated in these two domains for a model pressure of 15 kbar using three calibrations of the two-pyroxene thermometer (Bertrand & Mercier, 1985; Brey & Köhler, 1990; Taylor, 1998), the Ca-in-orthopyroxene thermometer (Brey & Köhler, 1990) and the Al-in-orthopyroxene thermometer (Witt-Eickschen & Seck, 1991), The results are given in Table 8 and are illustrated in Fig. 16. In spite of the common systematic differences between the values calculated using various thermometers, the results are comparable for all samples. The average temperatures range between 1040 and 1080 °C and they are reasonably similar for host peridotite and Zone I which supports equilibration of Zone I with host peridotite under comparable conditions. Similar equilibration temperatures were obtained for most symplectite-free xenoliths from Zinst (our unpublished data and Huckenholz and Kunzmann, 1993). Re-equilibration of the xenolith mineral assemblages at 1000-1100°C has been reported from other parts of the CEVP (e.g., Witt-Eickschen, 1997, Christensen et al. 2001, Matusiak-Małek et al. 2010, Puziewicz et al. 2011) and suggest a regional-scale heating of the upper mantle in the Tertiary.

In symplectites, the application of thermometers is more problematic. Zone III contains rare clinopyroxene and the assemblage Opx+Cpx+Spl is locally developed while the Opx+Spl±Pl assemblage dominates. In Zone II primary clinopyroxene was observed in one sample only. Both large variations in mineral chemistry and textures suggest rapid growth during formation of the fine grained Zone III symplectite. Furthermore, the chemistry of the reacting system differs substantially from that of peridotite, for which the thermometers were calibrated. These features can introduce significant errors in the temperature calculation. However, a high Al-content in both Opx and Cpx and a high Ca-content in Opx in the symplectite indicate generally high temperatures during their formation. The two-pyroxene and the Ca-in-orthopyroxene thermometers were applied assuming local equilibrium. The Al-in-orthopyroxene thermometer was not used, because the Al-contents of Opx significantly exceed the range for which it was calibrated. Also, the high variation of Al-content in orthopyroxene suggests that the effect of low diffusivity of Al in pyroxenes would introduce additional large errors (comp. Witt-Eickschen & Seck, 1991). The results show significant intra-sample variation of calculated temperatures and systematically higher values are obtained using the calibration of Taylor (1998) (Table 8 and Fig. 16). In spite of these variations and possible effects of the chemical composition of the reacting systems, the concordance of most temperature estimates suggests that the average calculated temperatures of 1190-1290°C reflect a real heating, likely responsible for the breakdown of garnet to form Zone III. The temperature increase in the order of 100-250 °C supports the multiphase evolution in different thermal conditions already suggested by the textural contrasts between the symplectites and host peridotite+Zone I. The generally high content of melt on grain boundaries throughout the samples discouraged us from using the element zoning in pyroxene rims as an independent indicator of late thermal evolution. The application of the Al-in-orthopyroxene barometer (Brey & Köhler, 1990) to Zone III was tested, but the results were rejected due to unacceptably large scatter.

This is a pre-copyedited, author-produced PDF of an article accepted for publication in Journal of Petrology *following peer review. The version of record* P. Špaček, L. Ackerman, G. Habler, R. Abart, and J. Ulrych: Garnet Breakdown, Symplectite Formation and Melting in Basanite-hosted Peridotite Xenoliths from Zinst (Bavaria, Bohemian Massif) J. Petrology (2013) 54 (8): 1691-1723 first published online May 31, 2013 doi:10.1093/petrology/egt028 *is available online at:* **http://petrology.oxfordjournals.org/content/54/8/1691**

8. DISCUSSION: GARNET BREAKDOWN HISTORY

The geometry of the above described pseudomorphs with generally spheroidal shape and concentric shell structure suggests that they were formed by breakdown of precursor garnet at static conditions, postdating ductile deformation of the peridotite. While the pyroxenes of Zone I are chemically and structurally equilibrated with the host lherzolite, the bulk composition of the symplectitic cores of the pseudomorphs remained close to that of garnet. Although partly obscured by later metasomatism, the primary mineral compositions indicate that the interface between the peridotite+Zone I and symplectite represented an important boundary between two largely closed chemical systems. Furthermore, in contrast to most earlier studies on kelyphitic coronae of garnet (see references below), our observations in the Zinst samples suggest that the formation of individual zones in the pseudomorphs reflect a multiphase evolution under changing conditions. Their origin seems to be largely independent and therefore they are considered separately in the following chapters.

8.1. REACTION OLIVINE + GARNET (ZONE I)

The mineral association Opx+Cpx+Spl is characteristic for coronae associated with garnet in peridotites, and it is usually interpreted in terms of the reaction

Grt + Ol → Opx + Cpx + Spl [1]

(e.g., Fiala 1966; Reid and Dawson, 1972; Godard and Martin, 2000; Obata 2011). This reaction was demonstrated experimentally (e.g., MacGregor, 1965; Kushiro & Yoder, 1966; Green & Ringwood, 1967, O'Hara et al., 1971). The origin of the coarse grained spinel-pyroxene clusters often observed in spinel peridotite xenoliths is debated in the literature, but it is mostly attributed to the same reaction (e.g., Smith, 1977; Medaris et al., 1997). Both fine grained kelyphite and coarse grained clusters typically form symplectites with intimate intergrowths of vermicular spinel and larger pyroxene grains (e.g., Medaris et al., 1997, Odashima et al. 2008, Obata 2011).

In the Zinst samples the reaction between former garnet and peridotite is corroborated by the systematic coincidence of coarse grained Zone I in the outer parts of the pseudomorphs and the fine grained symplectites with garnet composition in their centres. The mineral compositions and thermometry suggest that these clusters equilibrated with peridotite at 1040-1080°C. This is in the upper range of equilibration temperatures as inferred from other xenolith localities in the Bohemain Massif (Ackerman et al. 2007; Matusiak-Małek at al. 2010). However, symplectitic intergrowths are not developed in Zone I, which exhibits granular structure with equant pyroxenes and isolated spinel grains in interstitial positions instead, suggesting different mechanisms of primary crystallization or some later recrystallization. Furthermore, the widely ranging modal composition $Opx_{28\text{-}63(52)}$ $Cpx_{28\text{-}64(40)}$ $Spl_{7.5\text{-}17(9)}$ (molar ratios, medians in parentheses) differs from compositions observed by Smith (1977) or Medaris et al. (1997) (molar ratios $Opx_{51\text{-}59}$ $Cpx_{11\text{-}23}$ $Spl_{20\text{-}32}$) from which the origin by solid-state reaction [1] was inferred. In spite of a possible influence of errors in the calculation, the large variability in Cpx/Opx ratio and low content of spinel relative to the above described symplectitic intergrowths are clearly not compatible with the reaction Grt+Ol in a chemically closed system. Furthermore, as described above, in some samples Zone I is not developed or it is strongly reduced in volume and both pseudomorphs with and without Zone I are sometimes present in the same sample. Rare inclusions of olivine and clinopyroxene enclosed in Zones III and IV, both representing former garnet, lack specific reaction coronae at their interfaces. This indicates the crucial role of external liquids as mediators of reaction. These observations suggest that Zone I was formed as a product of

This is a pre-copyedited, author-produced PDF of an article accepted for publication in Journal of Petrology *following peer review. The version of record* P. Špaček, L. Ackerman, G. Habler, R. Abart, and J. Ulrych: Garnet Breakdown, Symplectite Formation and Melting in Basanite-hosted Peridotite Xenoliths from Zinst (Bavaria, Bohemian Massif) J. Petrology (2013) 54 (8): 1691-1723 first published online May 31, 2013 doi:10.1093/petrology/egt028 *is available online at:* **http://petrology.oxfordjournals.org/content/54/8/1691**

reaction [1] and its variability in terms of the volume and modal composition was controlled by non-uniform reaction progress due to inhomogeneous distribution of the mediating liquids and/or by later modification of the original reaction products in a chemically open system.
It is clearly seen, mostly in Type A pseudomorphs, that the width of Zone I is independent of the width of Zones II+III. Where Zone I is well developed, its volume is too large to be formed by transformation of the garnet now represented by Zones II+III since the small volume of the latter could not have provided enough Ca and Al for clinopyroxene and spinel in Zone I. This indicates that Zone I was formed prior to the symplectite and not simultaneously with it.

8.2. FORMATION OF KELYPHITES (ZONES II AND III)

The general appearance of Zones II+III is similar to a kelyphite typically developed in coronae around garnet in peridotites. Such kelyphites are generally explained as products of reaction between olivine and garnet (reaction 1 given above) and their structure is well described in reviews given by Godard and Martin (2000) and Obata (2011): in these cases, the outer, thinner, coarse grained shell consists mostly of orthopyroxene and is developed exclusively at the contact between the kelyphite and olivine. The inner, radially fibrous shell is sharply separated from the former, being composed of symplectitic vermicular intergrowths of fine grained pyroxenes, spinel and, in some cases, amphibole. As noted by Obata (2011), small, nodular, Cr-rich spinel grains occur sporadically near the boundary of the two shells.

However, the mineralogy and microstructure of both Zones II and III indicate that the kelyphites in the Zinst samples differ significantly from those commonly observed in peridotites and were likely formed by a different process. Zones II and III are largely uniform in lateral direction, both in terms of microstructure and mineral chemistry, and we did not observe any systematic variability related to adjacent olivine grains. Both zones are symplectites composed of Cr-poor spinel, Al-rich orthopyroxene and interstitial plagioclase. Spinel and orthopyroxene have similar compositions which differ significantly from those observed in Zone I. The major and trace element local bulk compositions of the pristine inner parts of the symplectite, including Zone IIIa and IV, are compatible with garnet and hence they are interpreted as products of isochemical garnet breakdown in terms of reaction

Grt ($Prp_{72}Alm_{15}Grs_{13}$) → Opx + Spl + An [2].

This reaction is similar in principle to the breakdown of garnet demonstrated experimentally by Kushiro and Yoder (1966):

Grt (Prp_2Grs_1) → Opx + Cpx + Spl + An [3].

In our case, clinopyroxene is subsidiary or entirely missing due to the low grossularite content in the garnet (comp. Obata, 2011). In this respect, our interpretation is similar to that made by Mukhopadhyay (1991), Keankeo (2000) or Dégi et al. (2010) to explain the formation of kelyphitic rims aroud garnet in olivine-free pyroxenites and granulites. Reaction [3] occurred at 14 kbar and 1200°C in experiment by Kushiro & Yoder (1966), however, this can not be used as a pressure constraint in our samples because of the significantly different garnet composition.

The interstitial plagioclase exhibits zonation in chemical composition varying from anorthite in the inner Zone IIIa to labradorite/andesine in the outer part of the symplectite (MM and SM domains). This zonation is, however, probably due to late metasomatic overprint, as will be discussed further, and we suggest that the primary origin in terms of reaction [2] applies to the entirety of Zone III.

Definitive conclusions on the origin of Zone II can not be made due to the abundance of interstitial silicate or carbonate melt pockets which may have replaced clinopyroxene. Zone II is often missing

This is a pre-copyedited, author-produced PDF of an article accepted for publication in Journal of Petrology *following peer review. The version of record* P. Špaček, L. Ackerman, G. Habler, R. Abart, and J. Ulrych: Garnet Breakdown, Symplectite Formation and Melting in Basanite-hosted Peridotite Xenoliths from Zinst (Bavaria, Bohemian Massif) J. Petrology (2013) 54 (8): 1691-1723 first published online May 31, 2013 doi:10.1093/petrology/egt028 *is available online at:* **http://petrology.oxfordjournals.org/content/54/8/1691**

or, conversely, it rarely forms the whole symplectite in D-type pseudomorphs, indicating that Zones I and II developed independently or diachronously rather than synchronously as in case of the two shells typical for kelyphites referred to above. The often irregular and gradual boundary between the two zones suggests that Zone II may represent the outer parts of former fibrous symplectite of Zone III which experienced grain growth. Involvement of Cpx in the reaction is suggested by lobate boundaries of clinopyroxene grains adjacent to or forming inclusions within the symplectite. However, the mineral chemistries of Opx and Spl are similar in Zones II and III and we did not observe any large-scale chemical zoning across the symplectite which would compare to that described by Obata (1994) in plagioclase-garnet pyroxenite, therein interpreted as being due to local equilibria between the reacting garnet and clinopyroxene. In our samples the possible role of clinopyroxene in the formation of kelyphites is minor and limited to the very rims of the symplectites only.

Fluid-assisted melting and crystallization

In general, the mineral habits and geometrical relations in Zone III strongly indicate crystallization of the mineral phases from a liquid. The aggregates of sub-idiomorphic Opx+Spl intergrowths and interstitial, fine grained, polycrystalline anorthite may be regarded as cumulate textures crystallized from silicate melt. In such a model the symplectite microstructure would be formed by oriented growth of cotectic cumulus crystals of Opx and Spl. The anorthite-poor domains in Zone III could then represent a specific form of adcumulate where continuous growth of cumulus crystals displaced the intercumulus liquid towards the reaction front, leading to the observed segregation of anorthite into interstitials and pools near the Zone III/IV interface. It is interesting to note that, in terms of microstructure, the inner parts of Zone III adjacent to the reaction front strongly resemble the experimentally produced reaction coronae between basanite melt and orthopyroxene grains with radially oriented laths of olivine and interstitial silicic glass (Shaw, 1999).

Incongruent melting of garnet and partial crystallization of the melts was proposed by Hunter & Taylor (1982) as a mechanism of formation of kelyphitic coronae around garnet in megacrysts and lherzolite xenoliths in kimberlite from northern USA. In their samples, the quenched melt was present as interstitial pockets, mainly between the kelyphite and garnet, as larger pools within kelyphite and also within the garnet itself. However, the high alkali content in the glass evidenced that external metasomatic agents played a significant role in melt formation, which is not indicated in our samples.

We suggest crystallization from the melt as the mechanism producing the microstructures of Zone III in the Zinst samples. Whether this melt was formed by incongruent melting of garnet or partial melting of previously formed Opx+Spl+An±Cpx symplectite remains an open question. Primary hydrated minerals, as potential local sources of water, have never been found in the Zinst xenoliths. Nevertheless, a crucial role of external fluids in the progress of garnet breakdown is clearly indicated by the spatial confinement of the symplectites into coronae, their promontories and cracks. The isochemical nature of the reaction indicates that these fluids acted as catalysers rather than metasomatic agents. The nature and origin of these fluids could not be identifed, since the analytical techniques used failed to detect any fingerprints even in trace element compositional patterns.

8.3. SYN-VOLCANIC ISOCHEMICAL BREAKDOWN OF GARNET RELICS (ZONE IV)

The fine grained Zone IV is very similar in many aspects to kelyphites described in garnet granulites or garnet pyroxenites (e.g., Dégi et al., 2010; Mukhopadhyay, 1991). As shown above, the bulk compositions of the non-altered parts of the Zone IV (types IVa and IVb) symplectites are compatible with pyrope-rich garnet. A slight enrichment in Na can not be ruled out, but generally the Na-content

is close to the upper range for garnets from upper mantle peridotites. Zones IVa and IVb can be considered as the nearly pristine symplectites formed by isochemical breakdown of garnet, through reaction [2]. In patchy, coarsened domains a clear enrichment in Ca, Na and K relative to pristine types as well as an increase in An modal content is observed indicating infiltration of metasomatic fluids percolating along microcracks, similarly as interpreted by Dégi et al. (2010) in mafic granulite xenoliths.

Formation of Zone IV clearly postdates the crystallization of Zone III as evidenced by the geometry of microstructural sub-domains, which often mimic in great detail the boundaries between Zone III and Zone IV. No systematic grain coarsening in Zone IV was observed and the only increase in grain size is associated with the alkali-enriched domains.

The microstructure suggests that garnet was replaced by the symplectite assemblage at a sharp reaction front. The organization of the microstructure into domains with constant shape preferred orientation is supposed to result from a complex geometry of the reaction front. The shape preferred orientation of the symplectite phases (sub)perpendicular to the Zone III/Zone IV interface probably reflects oriented growth normal to the advancing reaction front. This feature was recently referred to as the „law of normality“ by Obata (2011), who ascribed it to minimization of the strain energy created during symplectite formation.

As described above, the veinlets spreading radially from Zone IV into peridotite are clearly associated with Zone IV and are never present around other types of pseudomorphs. We suggest that these veinlets were most likely formed by opening of extensional cracks produced by swelling due to the rapid replacement of relict garnet by symplectite. The termination of most veinlets at the Zone III/IV interface supports a model of multiple-domain breakdown of garnet relics. In the case of simple rim-to-core progress of the reaction front, the veinlets would be expected to penetrate deeper in the Zone IV.

8.4. METASOMATIC EVENTS AND FORMATION OF OLIVINE+PLAGIOCLASE ASSEMBLAGE

The microstructural observations clearly indicate that the metasomatic transformations did not occur in a single event but resulted from a complex sequence of processes. The melt infiltration and metasomatism apparently overlap with the formation of the symplectites, and can provide important information on relative timing of symplectite evolution and its pressure conditions. Distinguishing the pre-volcanic upper mantle metasomatic processes from those related to later interaction of the xenoliths with the host basanite is a crucial issue.

Early metasomatism

The mineral composition of MM and SM domains hosted in the outer parts of the symplectites indicates an interaction of rock samples with Na-rich metasomatic agents. The bulk compositions of melt pockets can be explained by mixing of in-situ (mainly anorthite+pyroxene) and external components (Na, Crb, P, K) in variable ratios. The K-enrichment is only minor and the bulk major element compositions of silicate melt pockets with high Al-Si-Na-contents and low contents of Mg-Fe-Ti-K are in contrast with the composition of host basanite (compare typical weight ratio Na_2O/K_2O of 4 in basanite and > 12 in melt pockets; Electronic Appendix 1).

The carbonate pockets, by their habits and mineral assemblage Crb+Ol±Apa±Gei±Cpx, resemble features from Svalbard xenoliths described by Ionov et al. (1993) and interpreted therein as a product of metasomatism by carbonate-rich fluids taking place in the upper mantle. The LREE and LILE enrichment and the abundance of apatite observed in our samples are often referred to as characteristic signatures of carbonate metasomatism in the mantle (e.g., Yaxley et al., 1991; Ionov et

This is a pre-copyedited, author-produced PDF of an article accepted for publication in Journal of Petrology *following peer review. The version of record* P. Špaček, L. Ackerman, G. Habler, R. Abart, and J. Ulrych: Garnet Breakdown, Symplectite Formation and Melting in Basanite-hosted Peridotite Xenoliths from Zinst (Bavaria, Bohemian Massif) J. Petrology (2013) 54 (8): 1691-1723 first published online May 31, 2013 doi:10.1093/petrology/egt028 *is available online at:* **http://petrology.oxfordjournals.org/content/54/8/1691**

al., 1993; Rudnick et al., 1993, Ionov et al., 1994). Together with the close textural relationship between Na-plagioclase and carbonate within the same pockets and the absence of hydrated mineral phase, these features suggest an interaction with Na-carbonate-rich, water-poor melt or fluid.

We conclude that the origin of MM and SM domains in the outer portions of the symplectites is most likely not primarily related to the interaction of the xenoliths with basanite. Whether the two types of domains reflect two distinct phases of metasomatism is a subject to research further. It is suggested that these features were formed in the upper mantle, prior to the entrainment of xenoliths in the host basanite.

Veining and late metasomatic reactions

Contrastingly to melt pockets in symplectite, the mineralogy of the radial veinlets with abundant ternary and alkali feldspars suggests that these could represent melts and fluids mostly derived from the host basanite. The number of veinlets which reach the xenolith margin in thin sections is generally low, but the situation may be different in 3D. The unusual composition of veinlets with high content of geikielite and apatite indicates that the formation of vein-filling material was complex. It is likely that the uptake of external components was partly accomodated by porous flow through the xenolith, at least in the early phases of vein formation. In one possible model the extensional cracks opening at the Zone IV/Zone III boundary act as a suction pump, the injected melts possibly derived from a multiple source (basanite, components from MM domains and symplectite in general) are mixed close to the symplectite and pushed forward to the prograding tip of the veinlet by new volumes of injected melt. The outward migration of the reactive melt and the chromatographic effect of its reaction with Opx result in progressively increasing equilibration of the melt with Opx towards the tip (see section 5.5 and Fig. 13).

The OP domains with vermicular intergrowths of Na-rich plagioclase and olivine replacing orthopyroxene (Fig. 14f) are developed within the aureoles of the veinlets cross-cutting the outer parts of symplectite. Absence of similar features in other domains suggests that the presence of a liquid phase and/or alkalis played the crucial role in the progress of the reaction. A similar assemblage Ol + Spl + Pl ± glass replacing garnet and the older Opx + Spl + Pl symplectite was also observed by Török et al. (2005) in garnet granulite xenoliths from the Pannonian Basin. Typically the modal Ol/Pl proportion is close to unity in the aggregates and the mineral assemblage is indicative of the reaction:

Al-Opx + Na-Ca-rich liquid (+ Al-Spl) → Pl + Ol (+ Cr-Spl) [4].

Essentially, this reaction is similar to the sub-solidus reaction between omphacite, enstatite and spinel studied experimentally by Green & Hibberson (1970) and analogous to the near-solidus reaction described by Walter & Presnall (1994) in the CaO-MgO-Al_2O_3-SiO_2-Na_2O chemical system:

Opx + Cpx + Spl + liquid → Fo + Pl [5].

In the case of Zinst samples, the liquid was likely a mixture of external and in-situ melts, which was not in equilibrium with the solid phases and might have also substituted the Cpx component.

8.5. MODEL OF GARNET BREAKDOWN ON A P-T PATH

The distinct microstructural and chemical features of individual zones in the pseudomorphs and the results of geothermometry suggest that they reflect a multiphase evolution of the samples under changing conditions, with contrasting rates of garnet breakdown. To understand this evolution in time and its relation to Tertiary volcanism we attempt to estimate a P-T path upon which our preferred model of the origin of individual zones of the pseudomorphs is presented (Fig. 17). It must be stressed, however, that in the absence of geobarometric data on equilibration/crystallization only

an approximate P-T path can be reconstructed, based on the observed metamorphic reactions, thermometry, and indirect considerations.

The formation of coarse grained Zone I around relatively large relics of garnet documents the passage of the samples from the garnet to the spinel stability field and its chemical and textural equilibration with the host lherzolite under conditions where garnet was metastable. The temperature of equlibration was calculated at 1040-1080°C. The slow and incomplete reaction of garnet suggests that it occured close above the boundary of the garnet/spinel stability fields, which lies between 15 and 20 kbar for the calculated range of temperatures (O'Hara et al., 1971; Green & Falloon, 1998). This P-T position fits the model geotherm constructed by Christensen et al. (2001) for the sub-volcanic lithosphere in the northern Bohemian Massif at the Oligocene/Miocene boundary (Fig. 17). Since the boundary of the garnet/spinel stability fields has a positive slope in the phase diagram, reaction [1] can be explained both as a result of heating and/or decompression. Regional heating as expected during rifting in the Paleogene and indicated by high equlibration temperatures estimated for spinel peridotite xenoliths in the Bohemian Massif, is the most likely cause for the formation of Zone I. A relation to earlier events, e.g. to the Permian extension of the Variscan orogen, seems unlikely, taking into account the equlibration of peridotite+Zone I at high-temperature conditions, which would be difficult to preserve on a cold geotherm for a long time.

The results of thermometric calculations performed on Zone III, indicate approximate temperatures of symplectite crystallization in a range of 1190-1290 °C. In the expected absence of pressure increase, the 100-250 °C increase in temperature apparently shifted the mineral assemblage even farther from the garnet stability field. However, the lack of textural and chemical equilibration between the lherzolite+Zone I and the symplectite indicates that no significant reaction between garnet and adjacent minerals occured. This suggests that the formation of the symplectite occured shortly (in geological timescale) before the volcanic eruption, most likely as a direct response to Tertiary magmatism. Local, fluid-assisted melting and crystallization was suggested above to explain the features of Zone III. The uneven distribution of Al in orthopyroxene reflects disequilibrium within the symplectite assemblage indicating rapid crystal growth and cooling. As indicated by inherited sub-structures of the Zone III/IV boundary in Zone IV and by the termination of radial veinlets at the Zone III/IV interface, the spatial extent of Zone III was defined prior to formation of Zone IV and veining.

Based on the above discussed interaction of the samples with volatile Na- and carbonate-rich, K-poor liquids we infer that the complex evolution of Zone III took place in the upper mantle largely prior to the entrainment of the xenolith in basanite. In our model this also applies to melting and recrystallization in Zone III. We admit, however, that some microstructural features in Zone III may have formed in later phases of the evolution and therefore the position of the Zone III field in Fig. 17 includes the pre-volcanic heating, wall-rock/melt interaction, as well as the early xenolith stage. The timing and conditions of formation of Zone II are poorely constrained, but we suggest that it was developed by recrystallization of Zone III in its outer parts. In most samples, represented by xenoliths containing Type B, C and D pseudomorphs, the garnet breakdown reaction has gone to completion at this phase of evolution.

The final, rapid breakdown of metastable relict garnet originated in multiple closely spaced nuclei throughout the whole grain (Zone IV in Type A pseudomorphs), leading to swelling, fracturing and formation of the radial veins spreading into the host lherzolite. Based on the Tfs+Pl-dominated vein fill, we interpret the formation of the Zone IV to be roughly synchronous with or post-dating the fragmentation of peridotite wall-rock and entrainment of xenoliths in the basanite melt. The formation of Ol+Pl intergrowths by reaction [4] indicates transition to the plagioclase peridotite stability field. Unfortunately, this pressure-sensitive reaction exhibits strong compositional dependence, with Na_2O/CaO ratio and normative plagioclase content being the most important factors (e.g., Green & Hibberson, 1970, Borghini et al., 2010). The studies available to date indicate

This is a pre-copyedited, author-produced PDF of an article accepted for publication in Journal of Petrology *following peer review. The version of record* P. Špaček, L. Ackerman, G. Habler, R. Abart, and J. Ulrych: Garnet Breakdown, Symplectite Formation and Melting in Basanite-hosted Peridotite Xenoliths from Zinst (Bavaria, Bohemian Massif) J. Petrology (2013) 54 (8): 1691-1723 first published online May 31, 2013 doi:10.1093/petrology/egt028 *is available online at:* **http://petrology.oxfordjournals.org/content/54/8/1691**

that the Fo+Pl assemblage is stable below pressures of 0.7-1.5 GPa near the solidi of variably depleted peridotites. In Fig. 17 we plot the plagioclase-out curves of Green & Falloon (1998), Walter & Presnall (1994) and Borghini et al. (2010; fertile peridotite) to approximate the lower and upper maximum-pressure limits for Fo+Pl intergrowth formation.

9. SUMMARY AND CONCLUDING REMARKS

• The locality of Zinst provided rare, symplectite-bearing xenoliths which were entrained in Tertiary basanite as garnet peridotites. Such samples are unique to Cenozoic volcanics in the Bohemian Massif and Central Europe, from where only mantle peridotites and pyroxenites completely equilibrated in spinel stability field have been reported so far.

• Several types of complex pyroxene-spinel-plagioclase intergrowths in the xenolith suite were interpreted to represent a sequence of multiple phases of garnet breakdown. These pseudomorphs provide a unique chance to study pre-volcanic transformation processes in the upper mantle and the interaction between garnet peridotite and melts/fluids both prior to formation of xenoliths and during their ascent. The individual microstructurally and chemically distinct concentric zones in the pseudomorphs document the discontinuous evolution of the samples under changing conditions, with increasing rates of garnet breakdown. Three main phases were distinguished:

1) Early reaction Grt+Ol related to regional heating in the uppermost mantle and possible small-scale lithospheric extension, both likely taking place in the early stages of Tertiary rifting. Partial re-equilibration of the rocks in the spinel peridotite stability field at 1040-1080°C.

2) Largely isochemical, fluid-mediated breakdown of garnet to kelyphite in a short period of heating by ~100-250°C. Progressive crystallization of Opx+Spl symplectite and interstitial anorthite from melts or fluids is indicated by internal microstructures of kelyphites. The subsequent partial metasomatism by Na-rich, K-poor, carbonate-bearing melts/fluids suggests that this phase of garnet breakdown occured largely prior to the formation of xenolith and its entrainment in basanite magma.

3) Rapid isochemical breakdown of rare garnet relics into Opx+Spl+An microsymplectite leading to local swelling and opening of radial veinlets which introduced alkali-rich melts of largely external origin. Metasomatic melting in the external parts of the symplectites resulted in local formation of Ol+Pl intergrowths at the expense of Opx. This phase of garnet breakdown is compatible with rapid decompression of basanite-hosted xenolith, immediately preceding the eruption in Oligocene.

• The observed absence of reaction between garnet and olivine during symplectite formation is a feature uncommon to garnet peridotites. The rapid quenching of the advancing garnet breakdown reaction front reveals clear separation of two independent processes in the formation of garnet corona, the purely isochemical breakdown of garnet preceding the element exchange with olivine or pyroxene in adjacent peridotite. Taking into account the high fluid content in the reaction system, this points to 1) significant contrast in the reaction kinetics of the two processes, and 2) a very short time span between the formation of kelyphite and the eruption. From this point of view the Na-carbonate metasomatism, which largely post-dated the formation of Zone III, likely took place within an „aureole“ of volatile melts/fluids penetration in the proximity of the basanite magmatic body.

• The in-situ melts suggested to explain the microstructural features in kelyphite zone (Zone III) can be provided by incongruent melting of garnet or by partial melting of earlier formed products of garnet breakdown. No relics of primary hydrated minerals were ever found in the xenoliths from Zinst and it is suggested that local melting in the kelyphite domains was assisted by water-poor fluids of external origin. In spite of that, garnet and/or its breakdown products seem to melt selectively and

preferrentially since clinopyroxene and spinel grains in host peridotite exhibit only local, thin resorption rims, largely associated with late infiltration of external melt into xenolith.

• The lack of pervasive chemical and textural re-equilibration of the rock with symplectites documents the existence of metastable domain in the uppermost, probably lithospheric, mantle beneath the Zinst locality in the Tertiary. As indicated by geothermometry, the P-T conditions in the upper mantle prior to the volcanic event were well above the solidus of H+C+O fluid-bearing, fertile lherzolite and close to the solidus of water-free, carbonated lherzolite (Wyllie, 1988; Falloon & Green 1990). Under these conditions garnet peridotite domains could have been easily destabilised by local advective heating and addition of fluids. Even though observed in very rare samples, the fusion of garnet, or its earlier reaction coronae, may represent an incipient stage of a more profound, regionally extensive transformation taking place near the base of the sub-volcanic lithosphere. If present, such partially molten domains would likely have a strong influence on the dynamics and extent of the upper-mantle magmatic process related to volcanism. The mechanical weakening in the partially molten domains of metastable garnet peridotite and the addition of in-situ melts to the alkalic melts of deeper origin might control the local segregation of fluids and magma and the build-up of the chamber supplying the volcanic eruption. The seismic properties of such „corroded" lithospheric domains could be similar to those of the astenosphere and these might therefore manifest as updomings of low velocity zone.

• Radial fracturing and veining related to swelling in the final phase of garnet breakdown is an efficient mechanism of destruction of pseudomorphs after garnet, since it introduces highly reactive melt to unstable mineral assemblage and may lead to fragmentation of the xenolith, bringing the pseudomorphs into direct contact with the host basalt.

On-line data

Electronic appendices can be downloaded at http://www.petrology.oxfordjournals.org. Extensive imagery on mantle xenoliths from the Bohemian Massif can be found in the web atlas at http://xenolith.ipe.muni.cz.

Acknowledgements

We thank Michael Abratis for bringing us to Zinst quarry, Radek Škoda and Martin Racek for assistance with EMP, and Gordon Medaris and David Dolejš for discussions on selected petrological problems. Masaaki Obata, Arne Willner, Auke Baarhorn and Reto Gieré are thanked for careful and constructive reviews. This research was supported by Czech Science Foundation project 205/09/1170 and ESF/MSMT project CZ.1.07/2.3.00/20.0052. G. Habler acknowledges funding by the Austrian Science Fund (FWF): I471-N19 as part of the International DMG-FWF funded Research Network FOR 741 D-A-CH.

REFERENCES

Ackerman, L., Mahlen, N., Jelínek, E., Medaris, G.Jr., Ulrych, J., Strnad, L., Mihaljevič, M., (2007). Geochemistry and evolution of subcontinental lithospheric mantle in Central Europe: evidence from peridotite xenoliths of the Kozákov volcano, Czech Republic. *J. Petrol.* **48**, 2235–2260.

Babuška, V. & Plomerová, J. (1992). The lithosphere in central Europe-Seismological and petrological aspects. *Tectonophysics* **207**, 141-163.

Babuška, V., Fiala, J. & Plomerová, J. (2009). Bottom to top lithosphere structure and evolution of western Eger Rift (Central Europe). *International Journal of Earth Sciences* **99**, 891-907.

Bertrand, P. & Mercier, J.-C. C. (1985). The mutual solubility of coexisting ortho- and clinopyroxene: toward an absolute geothermometer for the natural system? *Earth and Planetary Science Letters* **76**, 109-122.

Borghini, G., Fumagalli, P. & Rampone, E. (2010). The stability of plagioclase in the upper mantle: subsolidus experiments on fertile and depleted lherzolite*. Journal of Petrology* **51***,* 229-254*.*

Boynton, W.V. (1984). Cosmochemistry of the rare earth elements: meteorite studies. *In: Henderson P (ed.): Rare Earth Element Geochemistry.* Elsevier, Amsterdam, pp 63–114.

Brey, G. P. & Köhler, T. (1990). Geothermobarometry in four-phase lherzolites: II. New thermobarometers and practical assessment of existing thermobarometry. *Journal of Petrology* **31**, 1352-1378.

Cheval, F., Dautria, J.-M. & Girod, M. (1989): Les enclaves de lherzolite à grenat et spinelle du volcan burdigalien de Beaulieu (Bouches du Rhône): des témoins d'une remontée du manteau supérieur associé à l'ouverture du bassin océanique provençal. *Comptes Rendus de l'Académie des Sciences*, Série II **309**(12), 1309–1315.

Christensen, N. I., Medaris, L. G., Jr,Wang, H. F. & Jelínek, E. (2001). Depth variation of seismic anisotropy and petrology in central European litosphere: A tectonothermal synthesis from spinel lherzolite. *Journal of Geophysical Research* **106**, 645-664.

Dégi, J., Abart, R., Török, K., Bali, E., Wirth, R. & Rhede, D. (2010). Symplectite formation during decompression induced garnet breakdown in lower crustal mafic granulite xenoliths: mechanisms and rates. *Contrib. Mineral. Petrol.* **159**, 293–314.

Dèzes, P., Schmid, S.M. & Ziegler, P.A. (2004): Evolution of the European Cenozoic Rift System: interaction of the Alpine and Pyrenean orogens with their foreland lithosphere. *Tectonophysics* **389**, 1-33.

Dörr, W. & Zulauf, G. (2008): Elevator tectonics and orogenic collapse of a Tibetan-style plateau in the European Variscides: the role of the Bohemian shear zone. *Int. J. Earth. Sci.*, DOI 10.1007/s00531-008-0389-x.

Falloon, T.J. & Green, D.H. (1990). Solidus of carbonated fertile peridotite under fluid-saturated conditions. *Geology* **18**, 195-199.

Faryad, S.W., Dolejš, D. & Machek, M. (2009). Gernet exsolution in pyroxene from clinopyroxenites in the Moldanubian zone: constraining the early pre-convergence history of ultramafic rocks in the Variscan orogen. *J. metamorphic Geol*. **27**, 655-671.

Fediuk, F. & Fediuková, E. (1989). Ultramafic nodules in basalts from northern Moravia, Czechoslovakia. *Sbor. geol. věd*, Geologie **44**, 9-49. Prague. (in Czech with English summary)

Fiala, J. (1966). The distribution of elements in mineral phases of some garnet lherzolites from the Bohemian massif. *Krystalinikum* **4**, 31–53.

Fischer, T. & Horálek, J. (2003). Space-time distribution of earthquake swarms in the principal focal zone of the NW Bohemia/Vogtland seismoactive region: period 1985–2001. *J. Geodyn.* **35**, 125–144.

Franke, W. (2000). The mid-European segment of the Variscides: tectonostratigraphic units, terrane boundaries and plate tectonic evolution. In: Franke W, Haak V., Oncken O., Tanner D. (eds.) Orogenic processes: quantification and modelling in the Variscan Belt. *Geological Society London Special Publications* **179**, 35–61.

Geissler, W. H., Kämpf, H., Seifert, W. & Dulski, P. (2007): Petrological and seismic studies of the lithosphere in the earthquake swarm region Vogtland/NW Bohemia, central Europe. *Journal of Volcanology and Geothermal Research* **159**, 1-3, 33-69.

Goes, S., Spakman, W. & Bijwaard, H., 1999. A lower mantle source for Central European volcanism, *Science,* **286,** 1928–1931.

Godard, G. & Martin, S. (2000). Petrogenesis of kelyphites in garnet peridotites: a case study from the Ulten zone, Italian Alps. *J. Geodyn.* **30**, 117–145.

Granet, M., Wilson, M. & Achauer, U., (1995). Imaging a mantle plume beneath the Massif Central (France), *Earth Planet. Sci. Lett.* **136,** 281–296.

Green, D. H. & Falloon, T. J. (1998). Pyrolite: A Ringwood concept and its current expression, In: Jackson I. (ed.): *The Earth's Mantle: Composition, Structure and Evolution,* 311-380. Cambridge University Press.

Green, D.H. & Hibberson, W. (1970). The instability of plagioclase in peridotite at high pressure. *Lithos* **3**, 209-221.

Green, D.H. & Ringwood, A.E. (1967). The stability fields of aluminous pyroxene peridotite and garnet peridotite and their relevance in the upper mantle structure. *Earth and Planetary Science Letters* **3**, 151-160.

Heuer, B., Geissler, W.H., Kind, R. & Kämpf, H. (2006). Seismic evidence for asthenospheric updoming beneath the western Bohemian Massif, central Europe. *Geoph. Res. Lett.* **33**, L05311, doi:10.1029/2005GL025158

Horn, P. & Rohrmüller, J. (2005). Geological map with new K-Ar ages of Cenozoic volcanites. In: Kämpf, H., Peterek, A., Rohrmüller, J., Kümpel H.-J., Geissler, W.H. (Eds.) (2005): The KTB Deep Crustal Laboratory and the western Eger Graben. GeoErlangen 2005, 24.-29.09.2005. *Schriftenreihe Deutsche Gesellschaft Geowissenschaften* **40**, 37-108.

Horn, I., Rudnick, R.L. & McDonough, W.F. (2000). Precise elemental and isotope ratio determination by simultaneous solution nebulization and laser ablation-ICP-MS: application to U–Pb geochronology. *Chemical Geology* **164**, 281–301.

Huckenholz, H.G. & Kunzmann, T. (1993). Tertiärer Vulkanismus in bayerischer Teil des Egergrabens und des mesozoischen Vorlandes. *Bei. Z. Eur. J. Mineral.* **5**, 1–34.

Hunter, R.H. & Taylor L.A. (1982). Instability of garnet from the mantle: Glass as evidence of metasomatic melting. *Geology* **10**, 617-620.

Ionov, D. A., Dupuy, C., O'Reilly, S. Y., Kopylova, M. G. & Genshaft Y. S. (1993). Carbonated peridotite xenoliths from Spitsbergen: implications for trace element signature of mantle carbonate metasomatism. *Earth and Planetary Science Letters* **119,** 283–297.

Ionov, D.A., Hofmann, A.W. & Shimizu, N. (1994). Metasomatism-induced melting in mantle xenoliths from Mongolia. *J. Petrology* **35**, 753–785.

Keankeo, W., Taylor, W.R. & Fitzgerald, J.D. (2000). Clinoferrosilite bearing kelyphite: a breakdown product of xenolithic garnet, Delegate breccia pipes, New South Wales, Australia. *Mineral. Mag.* **64**(3), 469–479.

Kopecký, L. (1978). Neoidic taphrogenic evolution and young alkaline volcanism of the Bohemian Massif. *Sbor geol věd*, Geol (Prague) **31**, 91–107.

Kotková J., O'Brien, P. and Ziemann, M. A. (2011). Diamond and coesite discovered in Saxony-type granulite: Solution to the Variscan garnet peridotite enigma. *Geology* **39**, 667-670.

Kramer, W. & Seifert, W., (2000). Mafische Xenolithe und Magmatite im östlichen Saxothuringikum un westlichen Lugikum: Ein Beitrag zum Krustenbau und zur regional Geologie. *Z. Geol. Wiss* **28**, 133–156.

Kushiro, I. & Yoder, H. S., Jr. (1966). Anorthite–forsterite and anorthite–enstatite reactions and their bearing on the basalt-eclogite transformation, *J. Petrology* **7**, 337–362.

Lustrino, M. & Wilson, M. (2007). The circum-Mediterranean anorogenic Cenozoic igneous province. *Earth-Sci. Rev*. **81**, 1–65.

MacGregor I.D. (1965): Stability fields of spinel and garnet peridotites in the synthetic system MgO-CaO-Al2O3-SiO2. *Carnegie Institute Washington Yearbook* **64**, 134-135.

Matte, P., Maluski, H., Rajlich, P. & Franke, W., 1990. Terrane boundaries in the Bohemian Massif: result of large-scale Variscan shearing. *Tectonophysics* **177**, 151–170.

Matusiak-Małek, M., Puziewicz, J., Ntaflos, T., Grégoire, M. & Downes, H. (2010). Metasomatic effects in the lithospheric mantle beneath the NE Bohemian massif: A case study of Lutynia (SW Poland) peridotite xenoliths. *Lithos* **117**, 49-60.

McDonough, W.F. & Sun, S., 1995. The composition of the Earth. *Chemical Geology* **120**, 223–253.

Medaris, L.G., Wang, H., Jelinek, E., Mihaljevic, M. & Jakes, P. (2005). Characteristics and origins of diverse Variscan peridotites in the Gföhl Nappe, Bohemian Massif, Czech Republic. *Lithos* **82**, 1–23.

Medaris, L.G., Fournelle, J.H., Wang, H.F. & Jelinek, E., 1997. Thermobarometry and reconstructed chemical compositions of spinel-pyroxene symplectites: evidence for pre-existing garnet in lherzolite xenoliths from Czech Neogene lavas. *Russ. Geol. Geophys.* **38**, 260–268.

Mukhopadhyay, B. (1991). Garnet breakdown in some deep seated garnetiferous xenoliths from the central Sierra Nevada: petrologic and tectonic implications. *Lithos* **27**, 59–78.

O'Brien, P. (2000). The fundamental Variscan problem: high-temperature metamorphism at different depths and high-pressure metamorphism at different temperatures. In: Franke W., Haak V., Oncken O., Tanner D. (eds.): Orogenic processes: quantification and modelling in the Variscan Belt. *Geological Society London Special Publications* **179**, 35–61.

O'Hara, M.J., Richardson, S.W. & Wilson, G. (1971). Garnet-peridotite stability and occurrence in crust and mantle. *Contributions to Mineralogy and Petrology* **32**, 48–68.

Obata, M. (1994). Material transfer and local equilibria in a zoned kelyphite from a garnet pyroxenite, Ronda, Spain. *J. Petrol.* **35**, 271–287.

Obata, M. (2011). Kelyphite and symplectite: textural and mineralogical diversities and universality, and a new dynamic view of their structural formation**.** In Sharkov E.V.: *New Frontiers in Tectonic Research - General Problems, Sedimentary Basins and Island Arcs*, 93-122. DOI: 10.5772/20265.

Obata, M. & Ozawa, K. (2011). Topotaxic relationships between spinel and pzroxene in kelzphite after garnet in mantle-derived peridotites and their implications to reaction mechanism and kinetics. *Mineralogy and Petrology* **101**, 217-224.

Odashima, N., Morishita, T., Ozawa, K., Nagahara, H., Tsuchiyama, A. & Nagashima, R. (2008). Formation and deformation mechanisms of pyroxene-spinel symplectite in an ascending mantle, the Horoman peridotite complex, Japan: An EBSD study. *Journal of Mineralogical and Petrological Sciences* **103**, 1-15.

Pearce, N.J.G., Perkins, W.T., Westgate, J.W., Gorton, M.P., Jackson, S.E., Neal, C.R. & Chenery, S.P. (1997). A compilation of new and published major and trace element data for NIST SRM 610 and NIST SRM 612 glass reference materials. *Geostandards Newsletter* **21**, 115-144.

Pouchou, J.-L., and Pichoir, F. (1991). Quantitative analysis of homogeneous or stratified microvolumes, applying the model "PAP". In: Heinrich, K.F.J. & Newbury, D.E. (Eds.): Electron Probe Quantitation, **31-75**. Plenum Press, New York.

Prodehl, C., Mueller, St., Haak, V. (1995). The European Cenozoic Rift System. In: Olsen, K.H. (Ed.), Continental Rifts: Evolution, Structure, Tectonics. Developments in Geotectonics 25. Elsevier, Amsterdam, pp. 133– 212.

Puziewicz, J., Koepke, J., Grégoire, M., Ntaflos, T. & Matusiak-Małek, M. (2011). Lithospheric mantle modification during Cenozoic rifting in Central Europe: evidence from the Księginki nephelinite (SW Poland) xenolith suite. *J. Petrol.* **52**, 2107-2145.

Reid, A.M. & Dawson (1972). Olivine-garnet reaction in peridotites from Tanzania. *Lithos* **5**, 115-124.

Rudnick, R. L., McDonough, W. F. & Chappell, B. W. (1993). Carbonatite metasomatism in the northern Tanzanian mantle: petrographic and geochemical characteristics. *Earth and Planetary Science Letters* **114,** 463–475.

Schmädicke, E., Gose, J. & Will, T.M. (2010). The P–T evolution of ultra high temperature garnet-bearing ultramafic rocks from the Saxonian Granulitgebirge Core Complex, Bohemian Massif. *J. metamorphic Geol.* **28**, 489-508.

Schulmann, K., Konopásek, J., Janoušek, V., Lexa, O., Lardeaux, J.M., Edel, J.B., Štípská, P., Ulrich, S. (2009). An Andean type Palaeozoic convergence in the Bohemian Massif. *Comptes Rendus Geoscience* **341**, 266-286.

Shaw, C.S.J. (1999). Dissolution of orthopyroxene in basanitic magma between 0.4 and 2 GPa: further implications for the origin of Si-rich alkaline glass inclusions in mantle xenoliths. *Contrib. Mineral. Petrol.* **135**, 114-132.

Siebel, W., Trzebski, R., Stettner, G., Hecht, L., Casten, U., Hohndorf, A. & Muller, P. (1997). Granitoid magmatism of the NW Bohemian massif revealed: gravity data, composition, age relations and phase concept. *Geol. Rundsch.* **86**, Suppl., S45-S63.

Smith, D. (1977). The origin and interpretation of spinel-pyroxene clusters in peridotite. *Journal of Geology* **85**, 476-482.

Taylor, W.R. (1998). An experimental test of some geothermometer and geobarometer formulations for upper mantle peridotites with application to the thermobarometry of fertile lherzolite and garnet websterite. *Neues Jahrbuch für Mineralogie, Abhandlungen* **172**, 381-408.

Todt, W. & Lippolt, H.J., (1975). K-Ar Alterbestimmungen an Vulkaniten bekannter paläomagnetischer Feldrichtung II. Sachsen. *J. Geoph.* **41**, 641–650.

Török, K., Dégi, J., Marosi, Gy. & Szép, A. (2005) Reduced carbonic fluids in mafic granulite xenoliths from the Bakony–Balaton Highland Volcanic Field, W-Hungary. *Chem. Geol.* **223**, 93–108.

Ulrych, J., Pešek, J., Štěpánková-Svobodová, J., Bosák, P., Lloyd, F.E., von Seckendorff, V., Lang, M. & Novák, J.K. (2006). Permo–Carboniferous volcanism in late Variscan continental basins of the Bohemian Massif (Czech Republic): geochemical characteristic. *Chem Erde* **66**, 37–56.

Ulrych, J., Dostal, J., Adamovič, J., Jelínek, E., Špaček, P., Hegner, E. & Balogh, K. (2011). Recurrent Cenozoic volcanic activity in the Bohemian Massif (Czech Republic). *Lithos* **123**, 133-144.

Walter, M.J. & Presnall, D.C. (1994). Melting behavior of simplified lherzolite in the system CaO-MgO-Al2O3-SiO2-Na2O from 7 to 35 Kbar, *J. Petrol*. **35**, 329-359.

Weinlich, F.H., Bräuer, K., Kämpf, H., Strauch, G., Tesař, J. & Weise, S.M. (1999). An active subcontinental mantle volatile system in the western Eger rift, Central Europe: Gas flux, isotopic (He, C, and N) and compositional fingerprints. *Geochim. Cosmochim. Acta* **63**, 3653–3671.

Wilson, M. & Downes, H. (2006). Tertiary-Quaternary intra-plate magmatism in Europe and its relationship to mantle dynamics. In: Gee, D., Stephenson, R. (eds.) European Lithosphere Dynamics, *Geol. Soc. Lond. Mem*. **32**, 147-166.

Witt-Eickschen, G. & Kramm, U. (1997). Mantle upwelling and metasomatism beneath Central Europe: Geochemical and isotopic constraints from mantle xenoliths from the Rhön (Germany). *J. Petrol.* **38**, 479-493.

Witt-Eickschen, G. & Seck, H. A. (1991). Solubility of Ca and Al in orthopyroxene from spinel peridotite: An improved version of an empirical geothermometer. *Contributions to Mineralogy and Petrology* **106**, 431-439.

Wyllie, P.J. (1988). Solidus curves, mantle plumes, and magma generation beneath Hawaii. *Journal of Geophysical Research* **93**, 4171-4181.

Ziegler, P.A., Schumacher, M.E., Dèzes, P., van Wees, J.-D. & Cloething, S. (2006). Post-Variscan evolution of the lithosphere in the area of the European Cenozoic Rift System. In: Gee, D., Stephenson, R. (Eds.) European Lithosphere Dynamics, *Geol. Soc. Lond. Mem.* **32**, 147–166.

Yaxley, G.M., Crawford A.J. & Green D.H. (1991). Evidence for carbonatite metasomatism in spinel peridotite xenoliths from western Victoria, Australia. *Earth and Planetary Science Letters* **107**, 305-317.

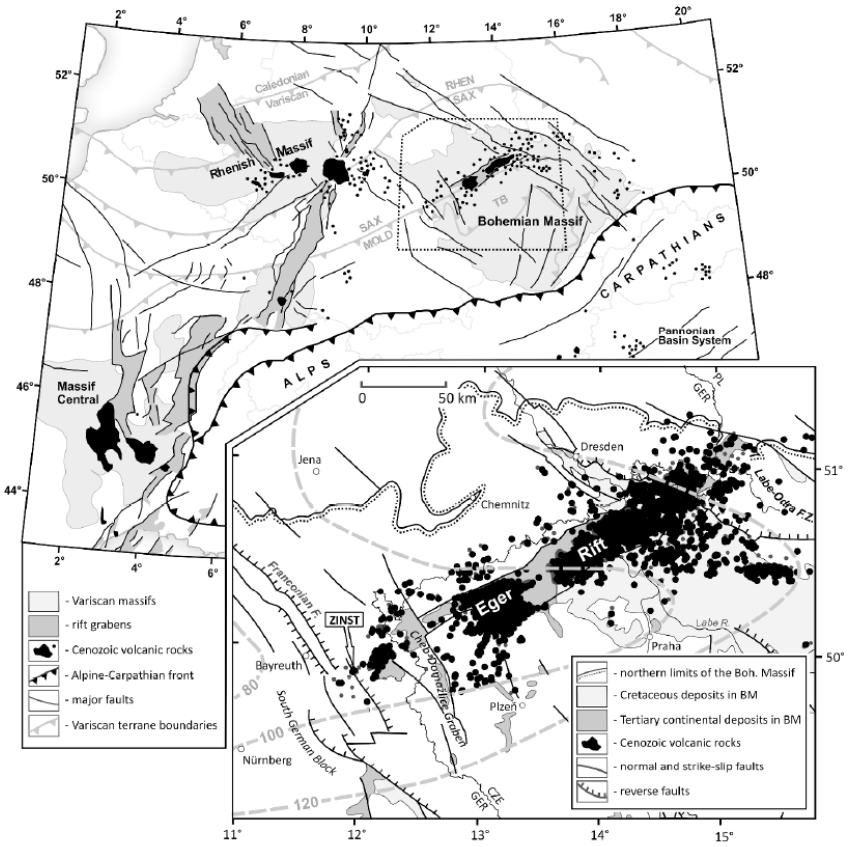

Fig. 1 Position of Zinst in the regional and supra-regional geological contexts. Top Schematic map of Central/Western Europe showing the grabens of the Cenozoic rift system (ECRIS), the Cenozoic volcanics (CEVP) and the Variscan massifs with terrane boundaries. The area shown in the bottom map is outlined by dotted line. Bottom Simplified map of the western Bohemian Massif and the Eger Rift. Zinst locality is indicated by the arrow. Dashed grey bold lines are isolines of the base of seismic lithosphere (thickness in kilometers) after Babuška and Plomerová (1992).

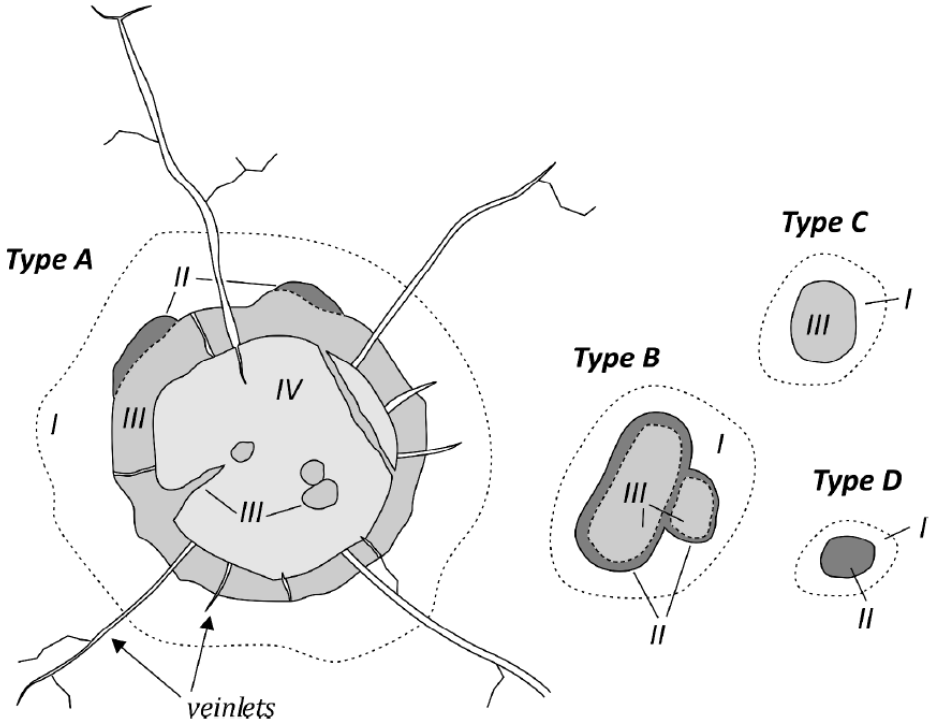

Fig. 2 Schematic diagram showing the basic geometry and typology of pseudomorphs after garnet in Zinst peridotites. Individual zones are marked by Roman numbers. Note that Zone I is developed in some pseudomorphs only. Also note that radial veinlets are only developed in association with Type A pseudomorphs (out of relative scale).

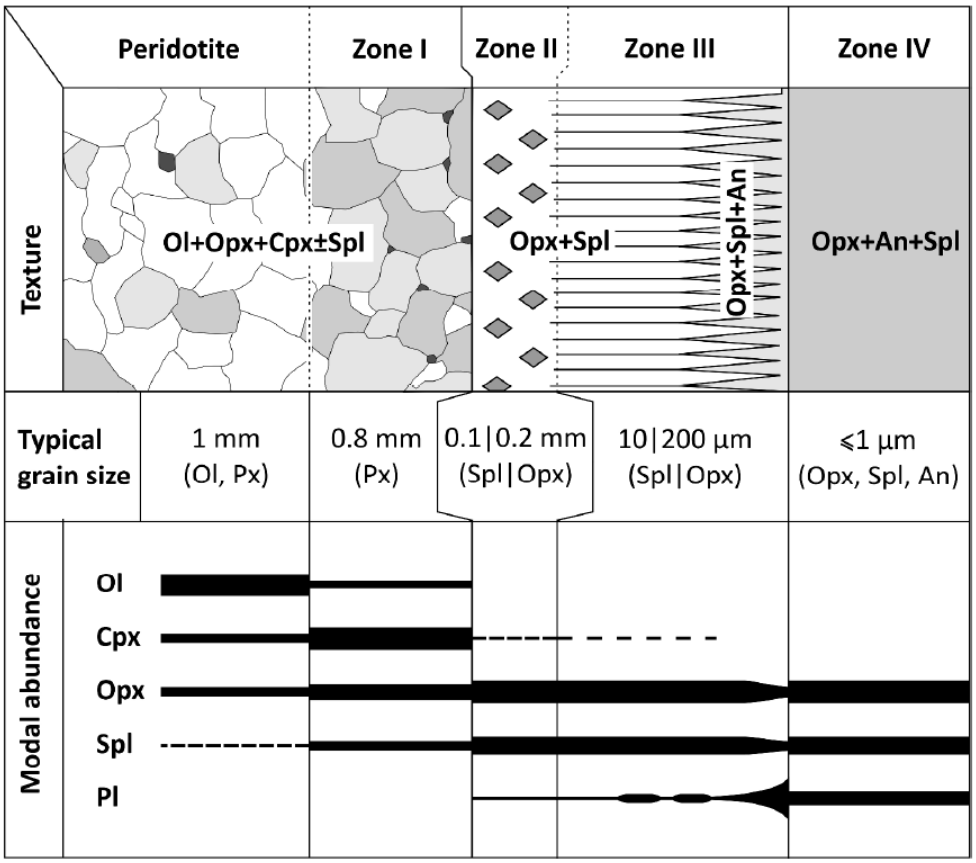

Fig. 3 Schematic, idealized diagram showing the mineral composition and basic textural features of the four zones of pseudomorphs after garnet and the host peridotites. Not to scale. Note that the structure and mineralogy of symplectite is independent on mineralogy of adjacent grains of Zone I. Zones II-IV are interpreted as late pseudomorphs after garnet while Zone I is interpreted as product of earlier reaction Ol+Grt. The local, late, melt-related features are not shown for sake of clarity.

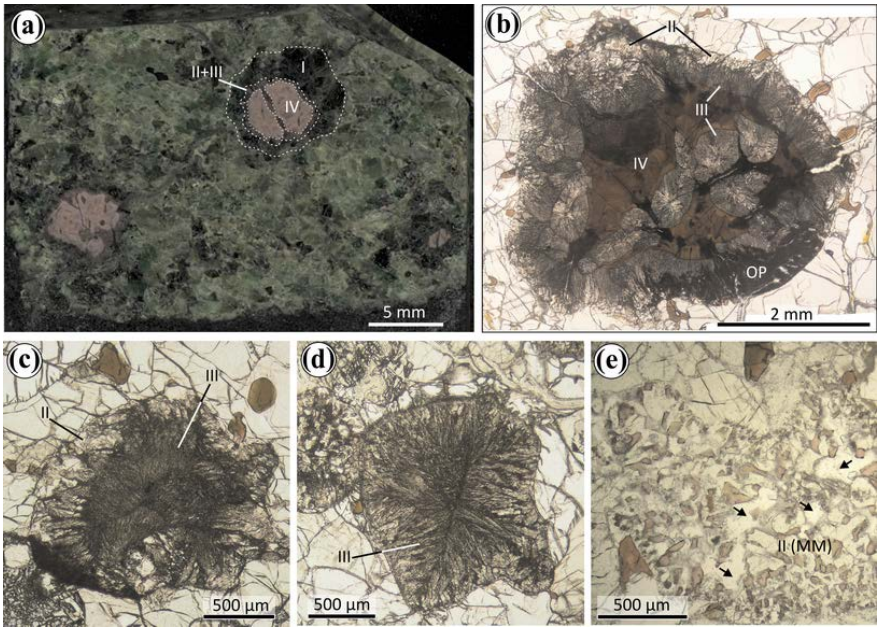

Fig. 4 Optical photomicrographs of pseudomorphs after garnet. Individual zones marked by Roman numbers I-IV; MM - metasomatic domains with melt pockets; OP - metasomatic domains with Ol-Pl intergrowths. a Polished rock slab with Type A pseudomorphs (reflected light). b Type A pseudomorph (photomosaic, ppl). c Type B pseudomorph (ppl). d Type C pseudomorph (ppl). e Type D pseudomorph with large carbonate melt pockets indicated by arrows (ppl).

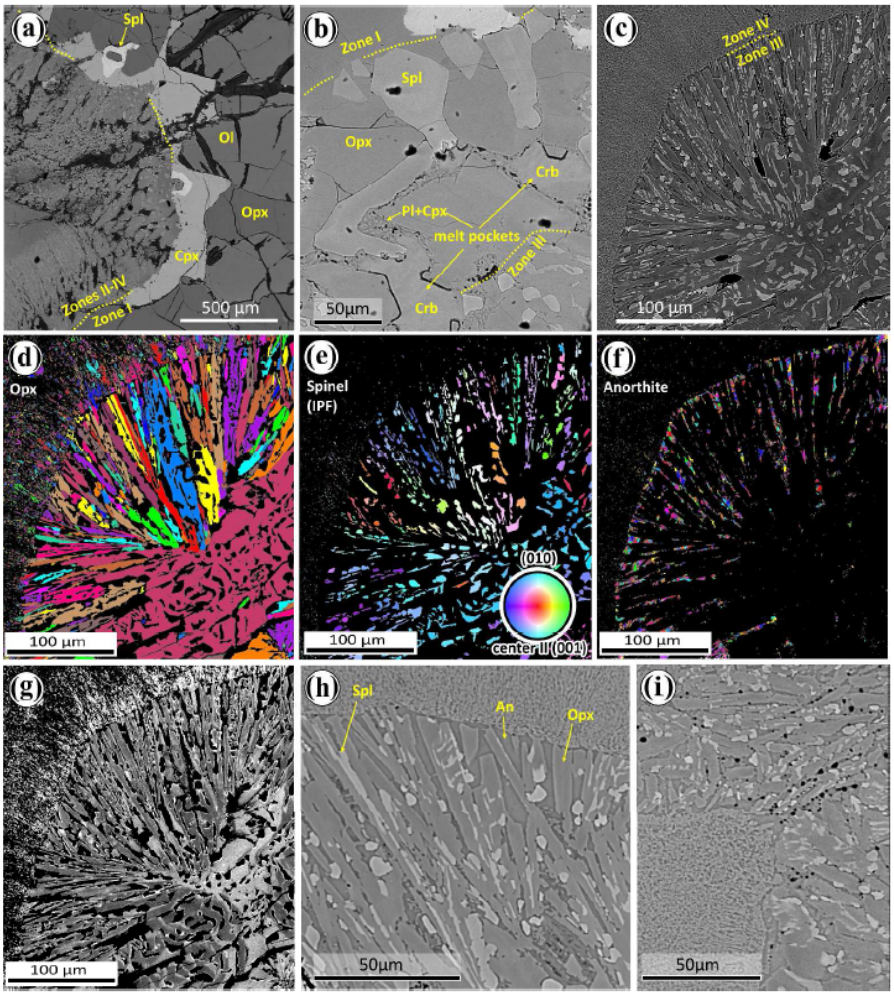

Fig. 5 Microstructure of Zones I-III of pseudomorphs after garnet. a Interface between Zone I and symplectite rimmed by crescent-shaped Cpx and atoll-shaped Spl (back-scatter electron image, BSE). b Zone II with symplectitic intergrowths of Opx+Spl and melt pockets (Pl+Cpx, Crb) (BSE). c Zone III („islet" enclosed in Zone IV) with radially fibrous symplectitic intergrowths of Opx+Spl and interstitial anorthite (BSE). d-f EBSD maps of Opx, Spl and An in Zone III (same area as in image c). In Opx and An maps individual grains with > 5° lattice misorientation across the grain boundaries are shown in different colours. In Spl map, inverse pole figure colour coding is used to show crystallographic orientations relative to the sample reference system (sample normal direction). Note the contrasting grain size of the three phases and the locally uniform crystallographic orientation of the individual spinel grain sections likely affiliated to larger grains with complex morphology. g Distribution map for Al in orthopyroxene of Zone III with brighter greyscale showing relatively higher Al-content (same area as in images c-d). Note the irregular intra-grain zonation. h Detail microstructure of Zone III near interface with Zone IV. Note the lamellar habits of Opx and some Spl grains (BSE). i Local concentration of bubble-shaped pores developed within interstitial anorthite in Zone III (BSE).

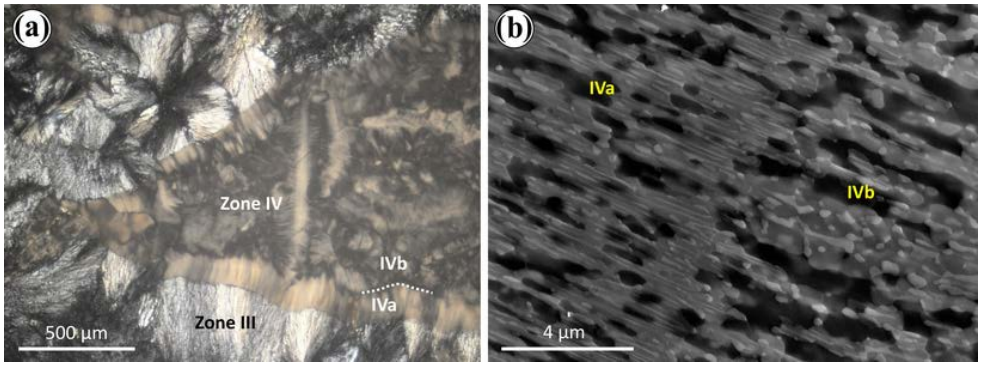

Fig. 6 Microstructure of Zone IV of pseudomorphs after garnet. a Optical photomicrograph (xpl) showing the domain sub-structure of the zone. Note the band of symplectite IVa tracing the Zone III/IV interface geometry. b SE image (FEG-SEM) showing in detail the microstructure of the two pristine subtypes of Zone IV.

Fig. 7

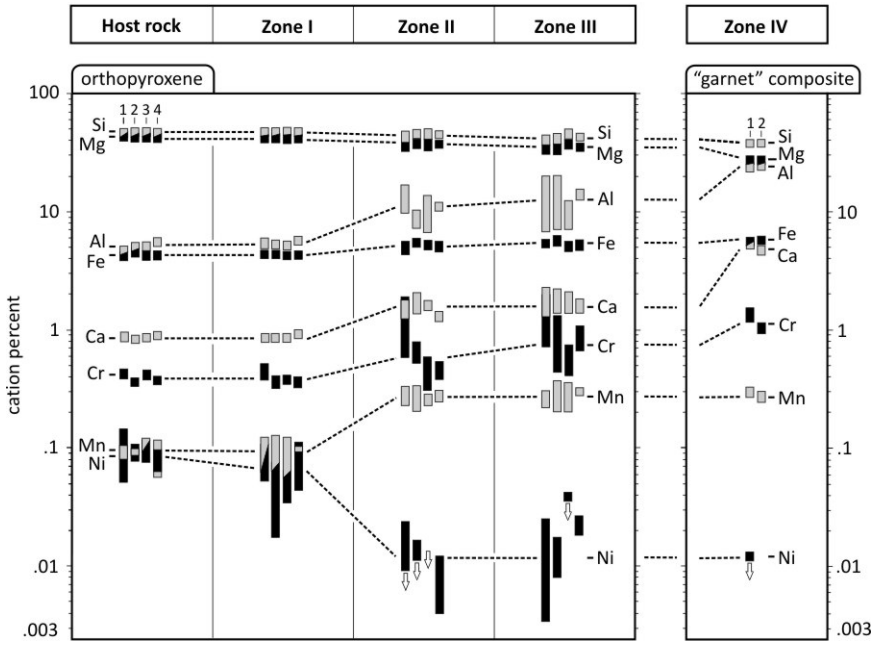

Fig. 7. Element distribution diagram of orthopyroxene in peridotite and Zones I–III of pseudomorphs after garnet (left) compared with element abundances in the fine-grained Zone IV with garnet bulk composition (right). Element contents are given in cation per cent on a logarithmic scale. The bars show the compositional range for representative samples with Type A pseudomorphs (1, ZIN2a; 2, ZIN50b) and Type B pseudomorphs (3, ZIN14; 4, ZIN56). Analyses with contents below the detection limits are indicated by arrows. The data for the same element are tied together by dashed lines. The major difference in element contents at the interface (peridotite + Zone I)/(Zone II + III), interpreted as the outer boundary of the garnet grain prior to formation of Zones II–IV, should be noted; also the general trends of element contents in orthopyroxene towards the composition of the former garnet now represented by Zone IV.

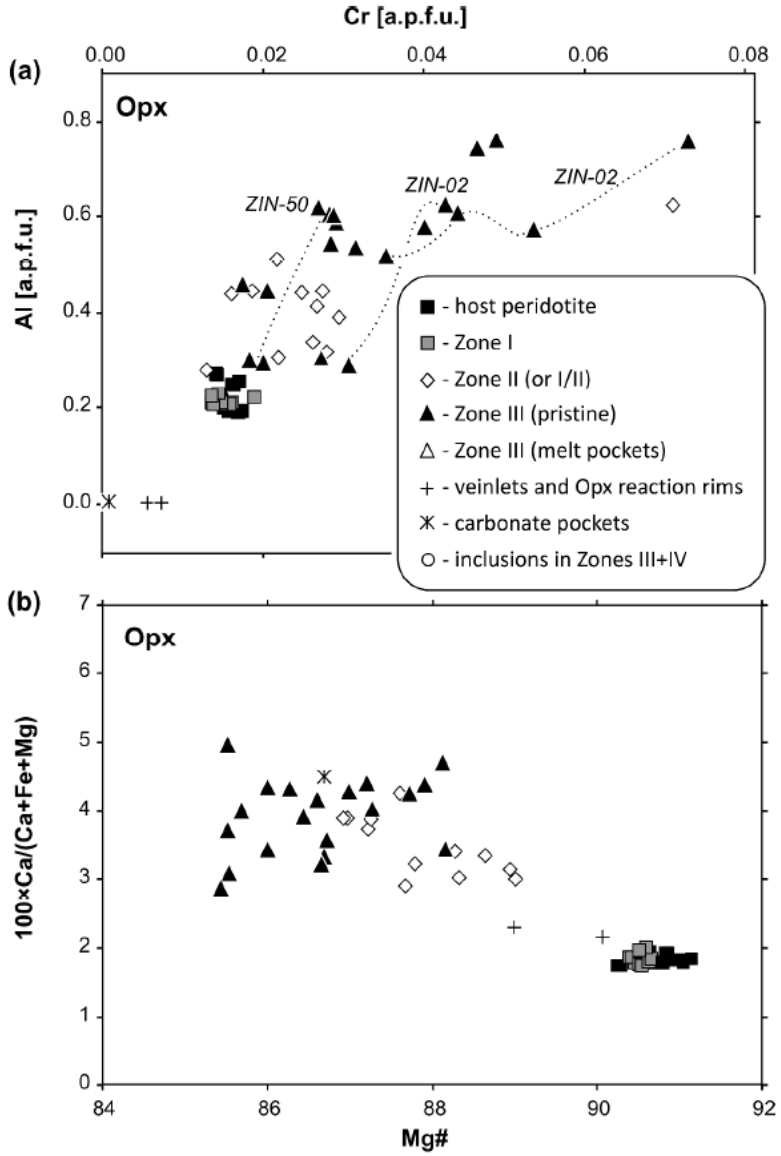

Fig. 8 Composition of orthopyroxene from „primary" and metasomatised domains shown in Al vs. Cr plot (a) and wollastonite molecule% vs. Mg# plot (b). Note the differences between host peridotite + Zone I and Zone III. Also note the large compositional variation within Zone III. The dotted lines join coexisting orthopyroxene grains from two samples with Type A pseudomorphs. The legend is universal for Figs. 8-11.

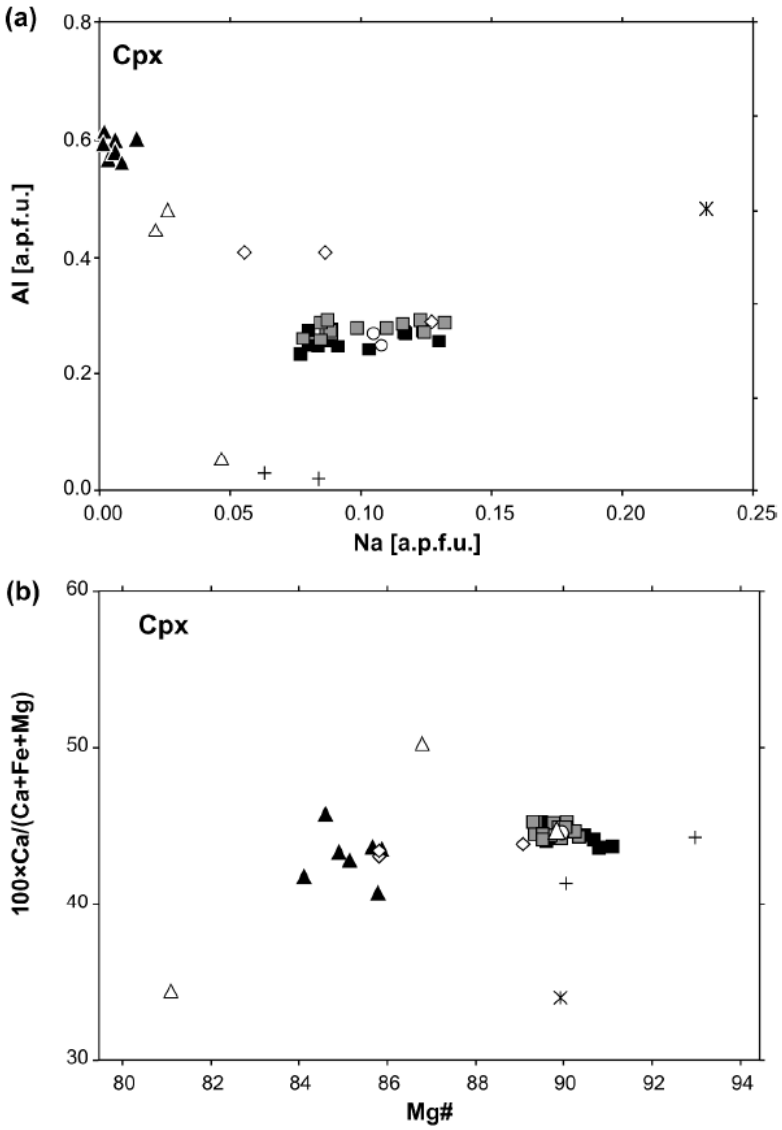

Fig. 9 Composition of clinopyroxene from "primary" and metasomatised domains shown in Al vs. Na plot (a) and wollastonite molecule% vs. Mg# plot (b). Symbols as in Fig. 8. Note the differences between host peridotite + Zone I and Zone III.

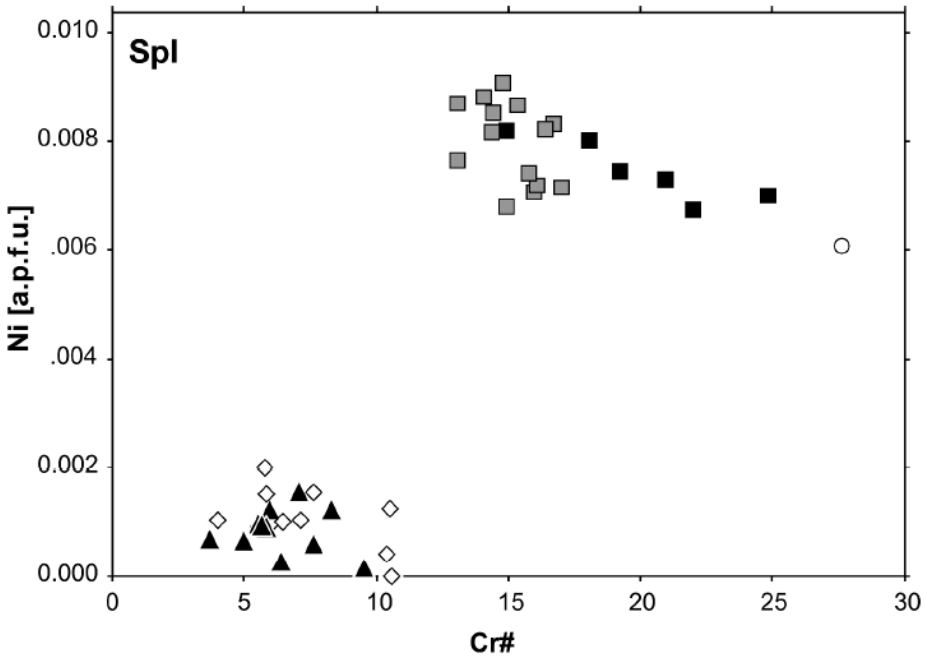

Fig. 10 Composition of spinel from "primary" and metasomatised domains shown in Ni vs. Cr# plot. Symbols as in Fig. 8. Note the differences between host peridotite + Zone I and Zones II + III.

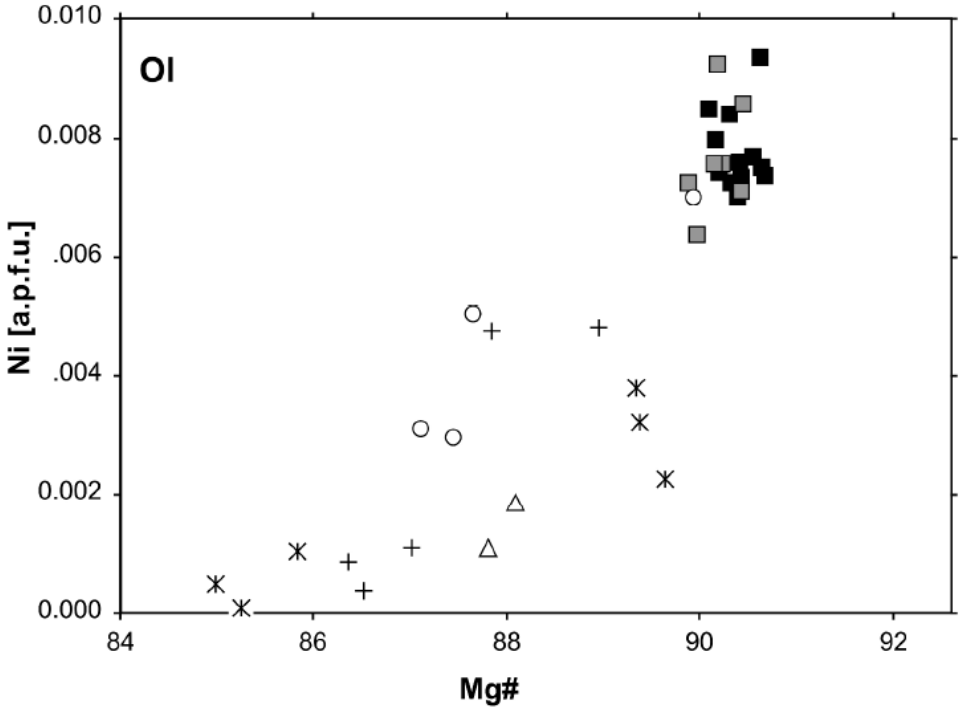

Fig. 11 Composition of olivine from "primary" and metasomatised domains shown in Ni vs. Mg# plot. Symbols as in Fig. 8.

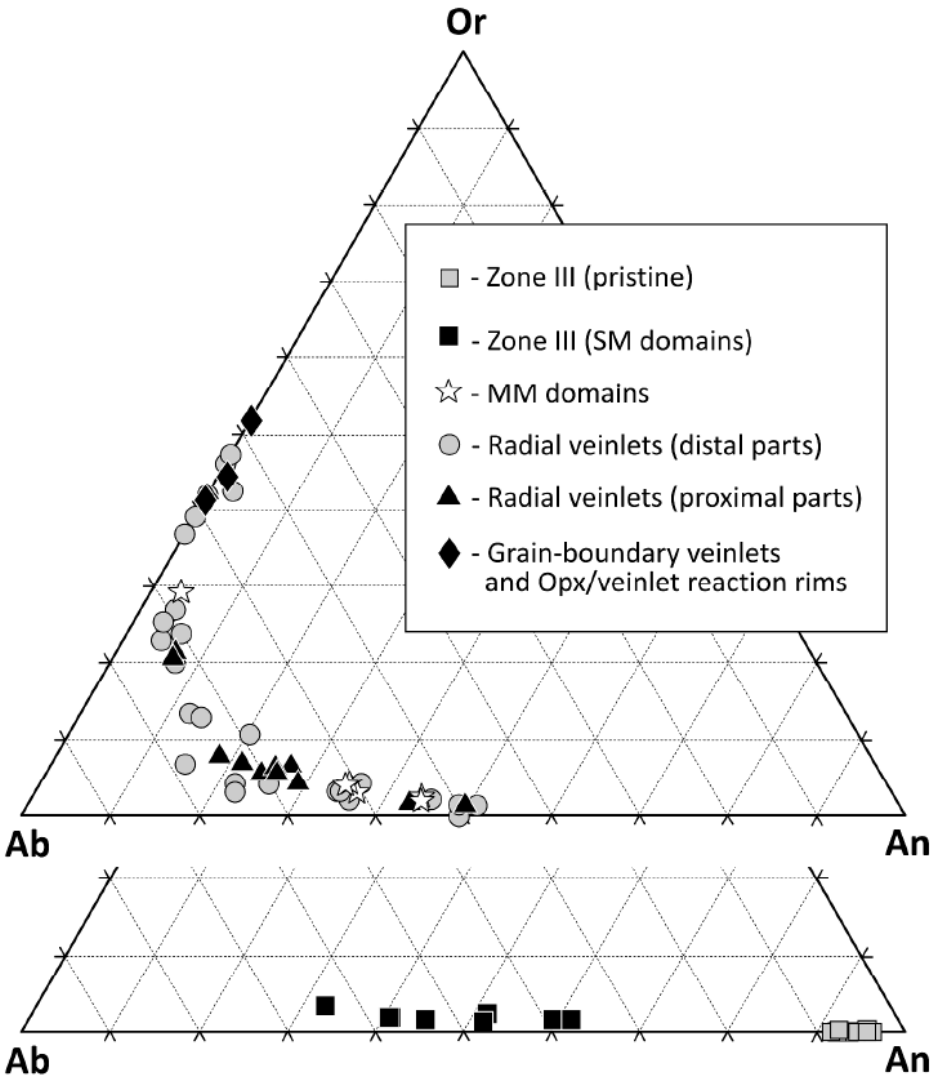

Fig. 12 Composition of feldspar from "primary" and metasomatised domains shown in ternary plot. Note the anorthitic composition of feldspar in the pristine, inner parts of Zone III. Also note the low content of orthoclase molecule in plagioclase of the metasomatised outer parts of Zone III (SM domains), contrasting with the abundance of ternary feldspar in veinlets.

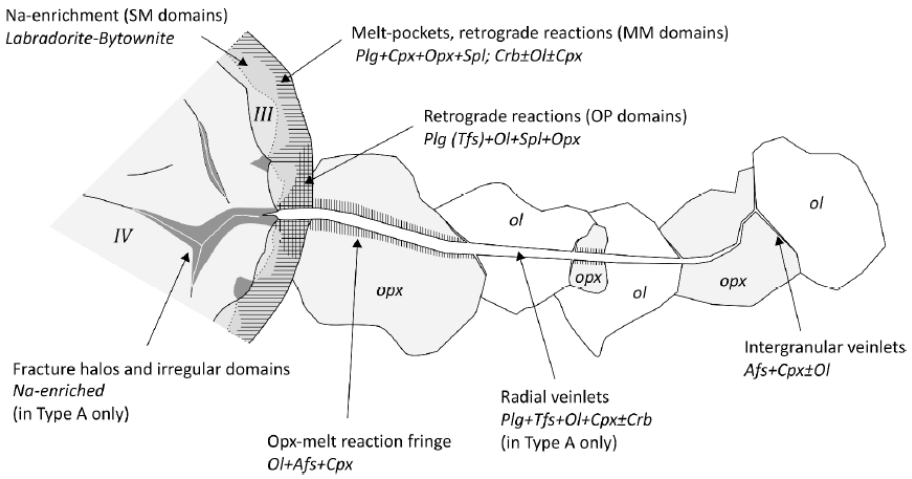

Fig. 13 Schematic diagram showing the morphological features of blind radial veinlets (associated with Type A pseudomorphs) and of domains in symplectite affected by late melt/fluid infiltration (partly common to all pseudomorph types). Major mineral assemblages characteristic for individual domains are also shown. Note the narrowing and fading-out of the Opx-melt reaction fringe in the outward direction from the symplectite. Not to scale.

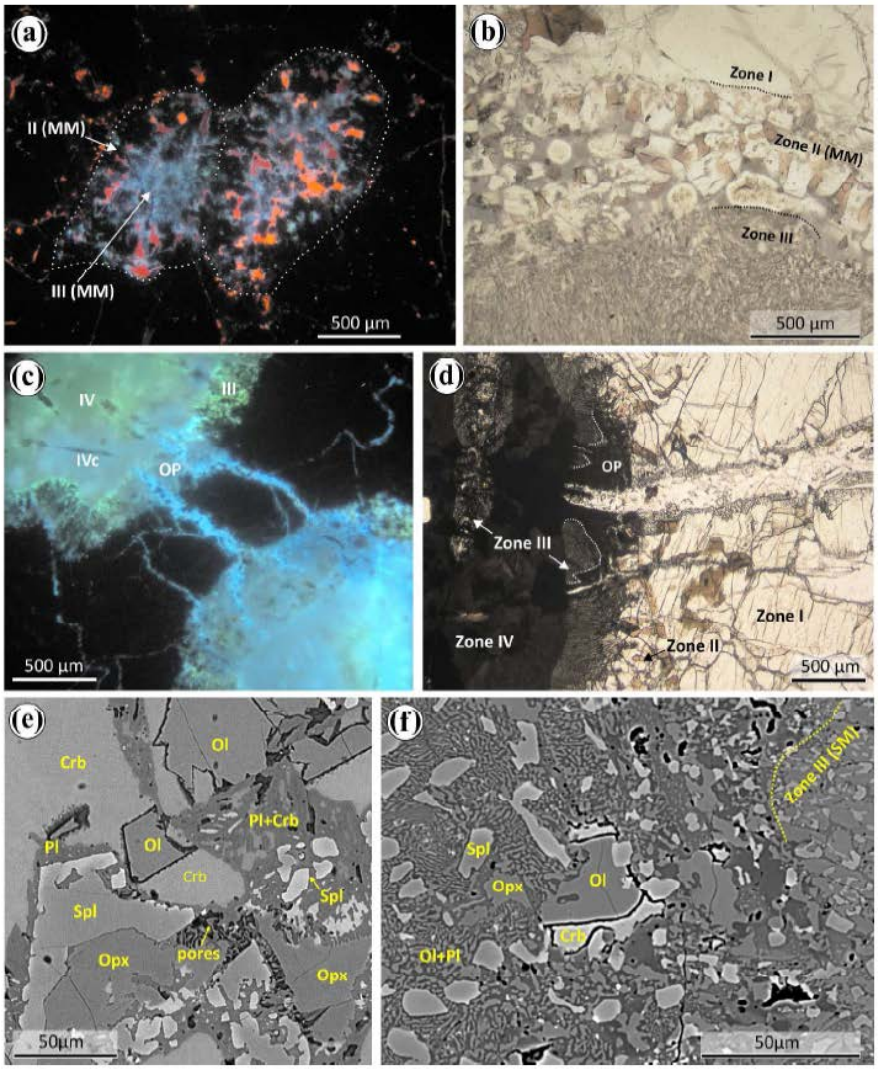

Fig. 14 Metasomatic features in samples with pseudomorphs after garnet. a CL image of strongly metasomatised Type B pseudomorph. Dotted line shows the extent of symplectite (Zones II+III). Blue corresponds to feldspar-rich domains, mainly present in Zone III. Bright orange is Fe-poor, dolomitic carbonate. Red and dull red are calcitic carbonate richer in Fe. b Optical image (ppl) of Zone II with abundant melt pockets and vesicles filled with chlorite. c CL image showing blind veinlets between two Type A pseudomorphs. Greenish colour corresponds to anorthite in pristine symplectites while cyan blue seems to reflect some additional metasomatic agents. d Characteristic termination of radial veinlet associated with Type A pseudomorph at Zone III/IV interface. OP - metasomatic domain with Ol+Pl intergrowths. e BSE image of melt pocket in outer symplectite. Note the close association of silicate and carbonate melts. f BSE image of OP domain with Ol+Pl intergrowths and Spl growing at the expense of Opx (left). Part of SM domain of Zone III is seen in the right.

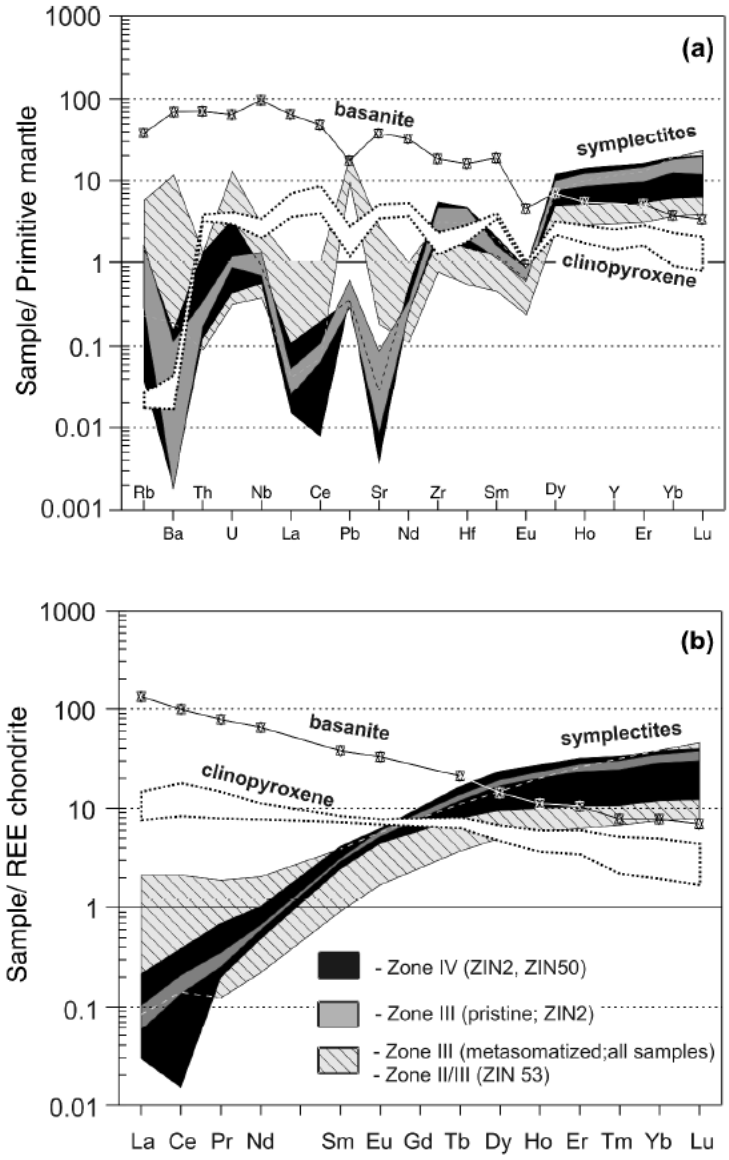

Fig. 15 Primitive mantle normalized trace element compositions (a) and chondrite normalized REE compositions (b) of Zone IV, pristine inner parts of Zone III and metasomatised outer parts of symplectite. Compositions of host basanite and of clinopyroxene in peridotite are shown for comparison. Note that the composition of pristine Zone III (grey field) is largely within the range of Zone IV (black field).

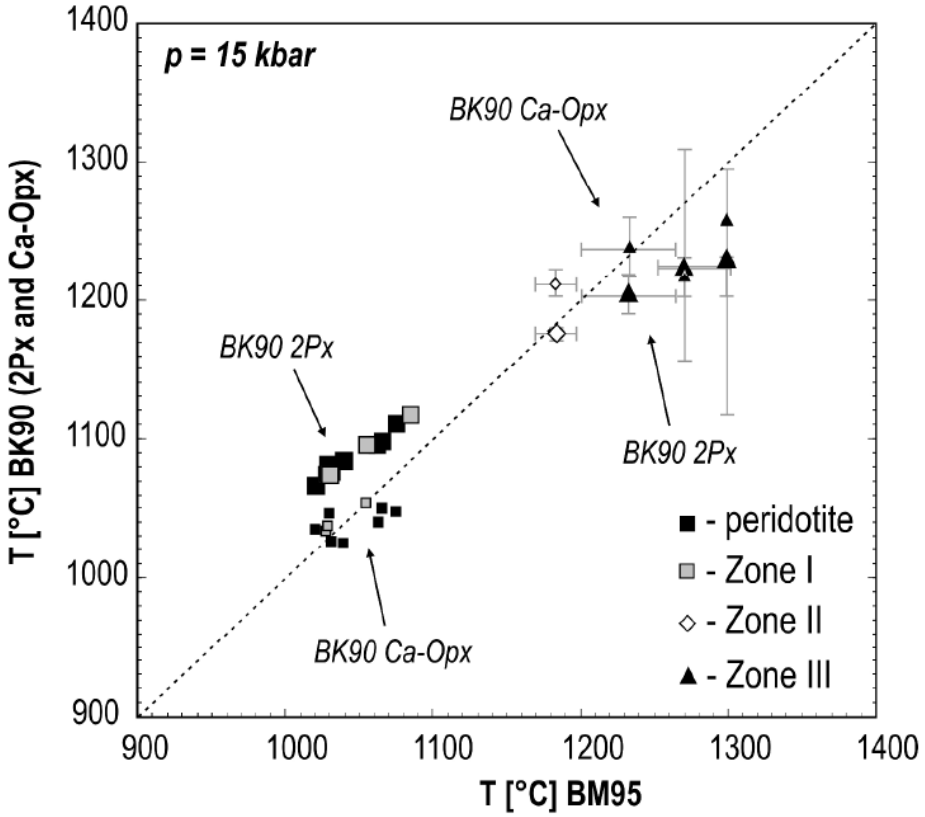

Fig. 16 Comparison of temperature estimates from the Bertrand and Mercier (1985) thermometer (abscissa) with those from two-pyroxene (large symbols) and Ca-in-orhopyroxene (small symbols) thermometers of Brey and Kohler (1990) (ordinate). Large variance in calculations for Zones II and III is shown by error bars (not shown for other domains for sake of clarity). Note the >100°C difference between the equilibration temperature of host rock + Zone I and the crystallization temperature in kelyphite.

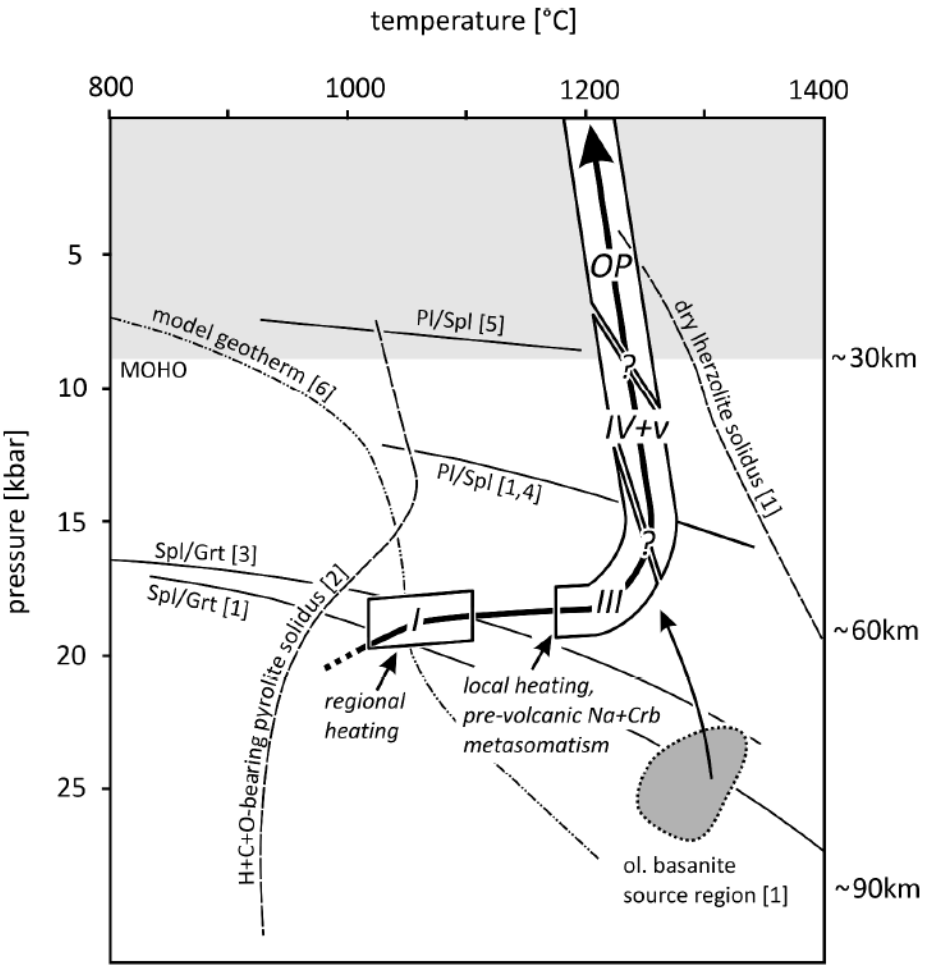

Fig. 17 Conceptual model of retrograde evolution of pseudomorph-bearing peridotites from Zinst xenoliths in P-T space. Zones of pseudomorphs after garnet described in text are indicated by Roman numbers I-IV; OP - metasomatic domains of outer symplectite with Ol+Pl intergrowths; v - radial silicate veinlets. Suggested regions of formation of individual zones are indicated along the P-T path approximated using experimental data and geothermometric data from this study. Oblique boundaries with question mark indicate uncertainty in P and T, not necessarily the overlap of the formation processes. Experimental solidi of dry and C-H-O-bearing lherzolites are shown (dashed lines) to illustrate that the reactions took place in the region where melting can occur, depending on fluid content and composition. Experimentally determined garnet and plagioclase stability field boundaries for lherzolite compositions are shown by solid curves. Dash-and-dot line shows a hypothetical geotherm modeled for Oligocene/Miocene lithosphere in northern Bohemian Massif. The xenolith exhumation path is approximated by 30°C/GPa liquid adiabat. Note that the pressure conditions of the reactions are generally not well constrained and the depth of the main bend in the P-T path in this diagram is largely controlled by the position of garnet stability field upper boundary (here the curve of [1] was preferred). [1] - Green and Falloon (1998), [2] - Falloon and Green (1990), [3] - O'Hara et al. (1971), [4] - Walter and Presnall (1994), [5] - Borghini et al. (2010; fertile lherzolite), [6] - Christensen et al. 2001.

This is a pre-copyedited, author-produced PDF of an article accepted for publication in Journal of Petrology *following peer review. The version of record* P. Špaček, L. Ackerman, G. Habler, R. Abart, and J. Ulrych: Garnet Breakdown, Symplectite Formation and Melting in Basanite-hosted Peridotite Xenoliths from Zinst (Bavaria, Bohemian Massif) J. Petrology (2013) 54 (8): 1691-1723 first published online May 31, 2013 doi:10.1093/petrology/egt028 *is available online at:* **http://petrology.oxfordjournals.org/content/54/8/1691**

Table 1 Representative major element compositions of orthopyroxene

Domain	perid.	perid.	Zone I	Zone I	Zone II	Zone II	Zone III	Zone III	Zone III	Zone III
Type	A	A	A	A	A	A	A	A	A	A
Sample	ZIN-02	ZIN-50	ZIN-02	ZIN-50	ZIN-02	ZIN-50	ZIN-02	ZIN-02	ZIN-50	ZIN-50
SiO_2	54.2	55.2	55.4	54.9	46.5	51.3	44.1	48.6	45.3	53.6
TiO_2	0.11	0.11	0.14	0.13	0.12	0.10	0.17	0.12	0.21	0.06
Al_2O_3	4.63	4.83	5.19	5.12	15.1	9.45	18.1	13.9	18.3	7.38
Cr_2O_3	0.62	0.52	0.60	0.55	2.56	1.07	2.60	1.95	1.76	0.67
FeO_{tot}	5.71	6.20	6.04	6.05	7.15	7.43	7.28	7.06	7.47	7.85
MnO	0.14	0.14	0.16	0.16	0.42	0.38	0.36	0.38	0.32	0.42
NiO	<0.09	0.14	0.13	<0.09	<0.09	<0.09	<0.09	<0.09	<0.09	<0.09
MgO	33.0	32.2	32.1	32.1	26.7	28.5	25.1	26.5	24.7	28.5
CaO	0.95	0.88	0.90	0.94	1.73	1.76	1.84	1.89	1.55	1.98
Na_2O	0.09	0.10	0.14	0.10	<0.09	<0.09	<0.09	<0.09	<0.09	<0.09
Total	99.5	100.4	100.8	100.2	100.4	100.2	99.8	100.5	99.9	100.5
Si	1.88	1.90	1.90	1.89	1.63	1.79	1.56	1.70	1.59	1.86
Ti	0.00	0.00	0.00	0.00	0.00	0.00	0.00	0.00	0.01	0.00
Al	0.19	0.20	0.21	0.21	0.62	0.39	0.76	0.57	0.76	0.30
Cr	0.02	0.01	0.02	0.01	0.07	0.03	0.07	0.05	0.05	0.02
Fe	0.17	0.18	0.17	0.17	0.21	0.22	0.22	0.21	0.22	0.23
Mn	0.00	0.00	0.00	0.00	0.01	0.01	0.01	0.01	0.01	0.01
Mg	1.71	1.65	1.64	1.65	1.40	1.48	1.32	1.38	1.30	1.47
Ca	0.04	0.03	0.03	0.03	0.07	0.07	0.07	0.07	0.06	0.07
Na	0.01	0.01	0.01	0.01	0.00	0.00	0.00	0.00	0.00	0.00
∑	4.01	3.99	3.99	3.99	4.02	3.99	4.02	3.99	4.00	3.98
Mg#	91.14	90.25	90.45	90.43	86.93	87.23	86.00	86.99	85.52	86.60
Wo	1.85	1.75	1.79	1.87	3.89	3.74	4.34	4.28	3.72	4.15
En	89.46	88.67	88.84	88.74	83.55	83.97	82.27	83.27	82.34	83.00
Fs	8.69	9.58	9.38	9.39	12.56	12.29	13.39	12.45	13.94	12.85

Oxides in wt%; Cations per 6 oxygen atoms; Wo=100×Ca/(Ca+Mg+Fe); En=100×Mg/(Ca+Mg+Fe); Fs=100×Fe/(Ca+Mg+Fe)

This is a pre-copyedited, author-produced PDF of an article accepted for publication in Journal of Petrology *following peer review. The version of record* P. Špaček, L. Ackerman, G. Habler, R. Abart, and J. Ulrych: Garnet Breakdown, Symplectite Formation and Melting in Basanite-hosted Peridotite Xenoliths from Zinst (Bavaria, Bohemian Massif) J. Petrology (2013) 54 (8): 1691-1723 first published online May 31, 2013 doi:10.1093/petrology/egt028 *is available online at:* **http://petrology.oxfordjournals.org/content/54/8/1691**

Table 2 Representative major element compositions of clinopyroxene

Domain	perid.	perid.	Zone I	Zone I	Zone I/II	Zone III	Zone III	Zone III	Zone III	MM (II)	MM (III)
Type	A	A	A	A	B	A	A	C	C	A	B
Sample	ZIN-02	ZIN-50	ZIN-02	ZIN-50	ZIN-14	ZIN-02	ZIN-50	zin 53 c	zin 53 c	ZIN-50	ZIN-14
SiO_2	51.4	52.6	51.9	52.2	51.1	46.9	47.3	47.0	47.5	52.1	48.0
TiO_2	0.38	0.38	0.43	0.41	0.35	0.26	0.44	0.29	0.30	0.47	1.13
Al_2O_3	5.75	6.45	6.42	6.68	9.70	13.1	14.0	14.5	14.1	6.9	11.2
Cr_2O_3	1.09	1.16	0.93	0.98	0.51	1.94	1.01	1.12	0.49	0.90	0.16
FeO_{tot}	2.98	3.20	3.07	3.26	3.99	4.28	4.97	4.59	4.48	3.41	4.51
MnO	0.07	0.10	0.11	0.15	0.28	0.44	0.35	0.35	0.30	0.12	0.24
NiO	0.09	<0.09	0.16	<0.09	<0.09	<0.09	<0.09	<0.09	<0.09	<0.09	<0.09
MgO	16.5	15.5	16.1	15.3	15.4	14.6	14.8	14.5	13.8	15.6	18.1
CaO	19.6	19.1	19.7	19.1	18.8	18.3	17.6	18.2	19.2	19.0	15.1
Na_2O	1.30	1.79	1.27	1.67	0.81	0.13	<0.09	<0.09	0.21	1.83	0.38
Total	99.4	100.7	100.3	100.0	101.1	100.2	100.6	100.8	100.6	100.6	99.0
Si	1.88	1.89	1.87	1.89	1.82	1.70	1.70	1.69	1.71	1.88	1.74
Ti	0.01	0.01	0.01	0.01	0.01	0.01	0.01	0.01	0.01	0.01	0.03
Al	0.25	0.27	0.27	0.28	0.41	0.56	0.60	0.62	0.60	0.29	0.48
Cr	0.03	0.03	0.03	0.03	0.01	0.06	0.03	0.03	0.01	0.03	0.00
Fe	0.09	0.10	0.09	0.10	0.12	0.13	0.15	0.14	0.14	0.10	0.14
Mn	0.00	0.00	0.00	0.00	0.01	0.01	0.01	0.01	0.01	0.00	0.01
Mg	0.90	0.83	0.87	0.83	0.82	0.79	0.79	0.78	0.74	0.84	0.98
Ca	0.77	0.74	0.76	0.74	0.72	0.71	0.68	0.70	0.74	0.73	0.59
Na	0.09	0.12	0.09	0.12	0.06	0.01	0.00	0.00	0.01	0.13	0.03
∑	4.02	4.00	4.01	4.00	3.98	3.98	3.97	3.98	3.98	4.01	4.00
Cr#	11.32	10.79	8.87	8.93	3.41	9.02	4.61	4.92	2.26	8.09	0.93
Mg#	90.82	89.61	90.36	89.34	85.81	85.87	84.11	84.91	84.60	89.06	81.09
Wo	43.65	44.22	44.28	44.50	43.41	43.57	41.84	43.40	45.74	43.89	34.48
En	51.18	49.99	50.35	49.58	49.41	48.45	48.92	48.06	45.90	49.97	57.48
Fs	5.17	5.79	5.37	5.91	7.18	7.97	9.24	8.54	8.36	6.14	8.04

Oxides in wt%; Cations per 6 oxygen atoms; Wo=100×Ca/(Ca+Mg+Fe); En=100×Mg/(Ca+Mg+Fe); Fs=100×Fe/(Ca+Mg+Fe)

Table 3 Representative major element compositions of spinel

Domain	perid.	perid.	Zone I	Zone I	Zone II	Zone II	Zone II	Zone III	Zone III	Zone III
Type	A	B	A	A	A	A	B	A	A	B
Sample	ZIN-02	ZIN-14	ZIN-02	ZIN-50	ZIN-02	ZIN-50	ZIN-14	ZIN-02	ZIN-50	ZIN-14
SiO_2	0.11	0.09	0.08	0.08	0.09	0.11	0.14	0.93	0.93	0.11
TiO_2	0.24	0.17	0.24	0.19	0.05	0.04	0.03	0.33	0.14	0.16
Al_2O_3	49.5	49.4	50.9	53.1	57.6	61.6	62.0	56.6	60.0	61.9
Cr_2O_3	16.3	17.6	15.2	13.0	10.0	5.37	5.75	8.87	5.67	5.53
FeO_{tot}	12.1	12.5	11.9	12.3	10.9	10.6	10.1	11.5	11.6	10.9
MnO	0.14	0.14	0.12	0.15	0.36	0.26	0.24	0.40	0.31	0.30
NiO	0.37	0.35	0.39	0.41	0.05	0.05	0.08	<0.04	0.06	0.05
MgO	19.3	20.3	19.7	19.7	19.4	20.3	21.6	18.8	19.4	20.8
CaO	<0.05	<0.05	<0.05	<0.05	<0.05	<0.05	<0.05	0.18	0.13	0.09
ZnO	<0.08	0.10	<0.08	0.08	<0.08	<0.08	<0.08	<0.08	<0.08	<0.08
V_2O_3	0.08	0.10	0.10	0.09	0.04	0.04	<0.04	0.04	<0.04	0.05
Total	99.4	100.7	98.8	99.0	98.6	98.4	100.0	98.9	98.2	99.9
Si	0.00	0.00	0.00	0.00	0.00	0.00	0.00	0.02	0.02	0.00
Ti	0.00	0.00	0.00	0.00	0.00	0.00	0.00	0.01	0.00	0.00
Al	1.58	1.54	1.60	1.66	1.78	1.87	1.85	1.77	1.84	1.85
Cr	0.35	0.37	0.32	0.27	0.21	0.11	0.11	0.19	0.12	0.11
Fe^{3+}	0.06	0.09	0.06	0.06	0.01	0.02	0.04	0.01	0.02	0.03
Fe^{2+}	0.21	0.19	0.20	0.21	0.23	0.21	0.18	0.24	0.24	0.20
Mn	0.00	0.00	0.00	0.00	0.01	0.01	0.01	0.01	0.01	0.01
Ni	0.01	0.01	0.01	0.01	0.00	0.00	0.00	0.00	0.00	0.00
Mg	0.78	0.80	0.79	0.78	0.76	0.78	0.81	0.74	0.75	0.79
Ca	0.00	0.00	0.00	0.00	0.00	0.00	0.00	0.01	0.00	0.00
∑	3.00	3.00	3.00	3.00	3.00	3.00	3.00	3.00	3.00	3.00
Cr#	18.08	19.28	16.74	14.09	10.46	5.52	5.86	9.52	5.96	5.66
Mg#	74.03	74.23	74.63	74.08	76.05	77.35	79.14	74.46	74.87	77.24

Oxides in wt%; Fe2+ and Fe3+ contents were calculated based on spinel stoichiometry.

Table 4 Representative major element compositions of olivine

Domain	perid.	perid.	Zone I	Zone I	OP	MM-Crb	MM-Crb	MM-Crb	vein
Type	A	A	A	B	A	A	B	B	A
Sample	ZIN-02	ZIN-56	ZIN-02	ZIN-14	ZIN-02	ZIN-02	ZIN-14	ZIN-14	ZIN-02
SiO_2	40.7	40.9	40.7	41.4	40.7	39.3	40.9	39.8	39.0
TiO_2	<0.03	<0.03	<0.03	<0.03	<0.03	<0.03	<0.03	<0.03	0.04
Cr_2O_3	<0.05	<0.05	0.06	<0.05	0.05	0.06	<0.05	<0.05	0.06
FeO_{tot}	9.27	9.47	9.21	9.49	11.4	13.7	10.0	13.3	12.7
MnO	0.12	0.16	0.10	0.13	0.54	0.60	0.33	0.55	0.59
NiO	0.36	0.40	0.36	0.39	0.09	<0.04	0.12	0.05	<0.04
MgO	49.6	48.8	49.3	49.2	47.4	45.5	48.6	45.3	46.0
CaO	0.10	0.07	0.06	0.11	<0.05	0.23	0.27	0.21	0.06
Total	100.3	99.9	99.8	100.8	100.2	99.6	100.4	99.3	99.2
Si	0.99	1.00	1.00	1.00	1.00	0.99	1.00	1.00	0.99
Fe	0.19	0.19	0.19	0.19	0.23	0.29	0.20	0.28	0.27
Mn	0.00	0.00	0.00	0.00	0.01	0.01	0.01	0.01	0.01
Ni	0.01	0.01	0.01	0.01	0.00	0.00	0.00	0.00	0.00
Mg	1.81	1.78	1.80	1.78	1.74	1.71	1.77	1.70	1.74
Ca	0.00	0.00	0.00	0.00	0.00	0.01	0.01	0.01	0.00
∑	3.00	3.00	3.00	2.99	2.99	3.01	3.00	3.00	3.01
Mg#	90.40	90.18	90.44	90.24	88.10	85.26	89.64	85.83	86.52

MM-Crb - carbonate bearing melt pocket; vein - radial silicate veinlet

Oxides in wt%; Cations per 4 oxygen atoms

Table 5 Representative major element compositions of feldspar

Domain	Zone III	Zone III	SM	SM	MM	MM	MM	vein	vein	RR
Type	A	A	A	A	A	B	B	A	A	A
Sample	ZIN-50	ZIN-50	ZIN-02	ZIN-02	ZIN-02	ZIN-14	ZIN-14	ZIN-02	ZIN-02	ZIN-02
SiO_2	43.9	44.1	55.8	56.9	55.2	57.1	57.8	60.8	63.5	65.9
Al_2O_3	35.2	35.5	27.0	25.7	27.9	26.9	26.9	23.6	21.8	18.9
FeO_{tot}	0.33	0.41	0.30	0.23	0.25	0.23	0.14	0.13	0.09	0.46
CaO	19.4	19.0	9.7	8.8	10.5	9.7	9.3	5.3	3.0	0.22
Na_2O	0.48	0.39	6.34	6.81	5.30	6.52	6.24	8.49	8.81	6.30
K_2O	<0.05	<0.05	0.25	0.35	0.23	0.38	0.42	1.06	2.33	7.84
BaO	<0.06	<0.06	<0.06	<0.06	<0.06	<0.06	<0.06	0.09	0.15	<0.06
SrO	<0.09	<0.09	<0.09	<0.09	0.09	<0.09	0.12	<0.09	0.12	<0.09
Total	99.4	99.5	99.3	98.8	99.5	101.2	101.1	99.8	99.8	99.6
Si	2.05	2.05	2.53	2.59	2.50	2.55	2.58	2.73	2.84	2.98
Al	1.94	1.95	1.44	1.38	1.49	1.42	1.41	1.25	1.15	1.01
Fe	0.01	0.02	0.01	0.01	0.01	0.01	0.01	0.01	0.00	0.02
Ca	0.97	0.95	0.47	0.43	0.51	0.47	0.44	0.26	0.15	0.01
Na	0.04	0.03	0.56	0.60	0.47	0.57	0.54	0.74	0.76	0.55
K	0.00	0.00	0.01	0.02	0.01	0.02	0.02	0.06	0.13	0.45
∑	5.01	4.99	5.03	5.03	4.99	5.03	5.00	5.04	5.03	5.02
An	95.60	96.45	45.09	40.77	51.59	44.32	44.12	24.30	14.01	1.07
Ab	4.24	3.53	53.50	57.32	47.07	53.65	53.52	69.96	73.25	54.39
Or	0.16	0.02	1.41	1.91	1.34	2.03	2.36	5.75	12.74	44.54

vein - radial silicate veinlet; RR - orthopyroxene-veinlet reaction rim
Oxides in wt%; Cations per 8 oxygen atoms

Table 6 Representative major element bulk compositions of fine grained symplectites in Zones III and IV with garnet affinity

Domain	Zone IV	Zone IV	Zone IV	Zone IV	Zone IVc	Zone III	Zone III	Zone III	Zone III
Sample	ZIN-02	ZIN-02	ZIN-50	ZIN-50	ZIN-02	ZIN-02	ZIN-02	ZIN-50	ZIN-50
SiO_2	41.9	41.8	41.4	41.6	40.9	42.7	42.7	38.9	40.2
TiO_2	0.21	0.17	0.19	0.17	0.10	0.22	0.22	0.16	0.19
Al_2O_3	21.9	21.7	22.5	22.5	21.7	21.8	20.2	21.9	20.2
Cr_2O_3	2.02	2.14	1.49	1.39	1.93	2.08	2.06	1.24	1.21
FeO_{tot}	7.46	7.10	7.49	7.61	6.53	7.09	7.51	7.06	6.99
MnO	0.40	0.34	0.36	0.36	0.29	0.35	0.45	0.34	0.36
MgO	20.0	20.2	20.1	20.0	18.6	19.6	21.9	19.6	20.0
CaO	5.39	5.29	4.90	5.10	7.67	5.62	4.30	4.83	4.61
Na_2O	0.17	0.28	0.29	0.22	1.75	0.21	0.17	0.17	0.25
Total	99.6	99.1	98.8	99.0	99.6	99.8	99.8	94.3	94.1
Si	3.00	3.01	2.99	2.99	2.99	3.05	3.05	2.94	3.04
Ti	0.01	0.01	0.01	0.01	0.01	0.01	0.01	0.01	0.01
Al	1.85	1.84	1.91	1.91	1.87	1.83	1.70	1.95	1.80
Cr	0.11	0.12	0.09	0.08	0.11	0.12	0.12	0.07	0.07
Fe^{3+}	0.02	0.03	0.00	0.00	0.01	0.04	0.17	-0.03	0.12
Fe^{2+}	0.43	0.40	0.47	0.45	0.39	0.38	0.28	0.48	0.32
Mn	0.02	0.02	0.02	0.02	0.02	0.02	0.03	0.02	0.02
Mg	2.14	2.16	2.16	2.14	2.02	2.08	2.34	2.21	2.26
Ca	0.41	0.41	0.38	0.39	0.60	0.43	0.33	0.39	0.37
∑	8.00	8.00	8.00	8.00	8.02	7.97	8.03	8.04	8.02
Prp	0.71	0.72	0.72	0.71	0.67	0.71	0.79	0.71	0.76
Alm	0.14	0.13	0.15	0.15	0.13	0.13	0.09	0.15	0.11
Grs	0.14	0.14	0.13	0.13	0.20	0.15	0.11	0.13	0.13
Sps	0.01	0.01	0.01	0.01	0.01	0.01	0.01	0.01	0.01

Oxides in wt%; Cations per 12 oxygen atoms (assumed garnet composition)

This is a pre-copyedited, author-produced PDF of an article accepted for publication in Journal of Petrology *following peer review. The version of record* P. Špaček, L. Ackerman, G. Habler, R. Abart, and J. Ulrych: Garnet Breakdown, Symplectite Formation and Melting in Basanite-hosted Peridotite Xenoliths from Zinst (Bavaria, Bohemian Massif) J. Petrology (2013) 54 (8): 1691-1723 first published online May 31, 2013 doi:10.1093/petrology/egt028 *is available online at:* **http://petrology.oxfordjournals.org/content/54/8/1691**

Table 7 Representative trace element compositions (in ppm) of Zone IV, pristine inner parts of Zone III and metasomatised outer parts of symplectite

Feature	**pristine symplectite**				**metasomatised domains**				**Cpx**	**host basanite**
Domain	**Zone IV**	**Zone IV**	**Zone III (fine gr.)**	**Zone III (coarser)**	**SM/MM (Zone III)**	**MM (Zone III)**	**OP (Zone III)**	**vein aureole**		
Sample	ZIN-50	ZIN-02	ZIN-02	ZIN-02	ZIN-50	ZIN-50	ZIN-02	ZIN-02	ZIN-02	B-10
Li	0.66	7.2	3.5	9.3	6.3	31	10	37	49	6.0
Rb	0.038	0.83	0.16	0.47	0.56	3.3	1.6	494	0.013	23
Sr	0.067	0.17	0.62	1.6	13	30	53	219	77	754
Y	24	34	30	37	16	30	26	13	11	20
Zr	20	45	25	40	11	24	32	45	25	192
Nb	0.39	0.41	0.58	0.43	0.97	1.8	1.6	27	1.8	64
Ba	<0.032	0.012	0.20	0.70	10	33	74	254	0.052	455
La	0.010	0.019	0.021	0.018	0.10	0.50	0.66	11	3.2	42
Ce	0.11	0.15	0.12	0.12	0.21	1.4	1.7	27	10	82
Pr	0.029	0.043	0.029	0.042	0.028	0.13	0.23	3.1	1.4	10
Nd	0.34	0.48	0.28	0.37	0.21	0.56	1.2	12	6.3	40
Sm	0.47	0.74	0.44	0.57	0.25	0.45	0.76	2.3	1.6	7.6
Eu	0.32	0.46	0.33	0.38	0.18	0.32	0.42	0.68	0.57	2.5
Tb	0.44	0.63	0.47	0.57	0.26	0.43	0.49	0.44	0.39	1.0
Dy	3.8	5.7	4.7	5.5	2.4	4.2	4.3	2.2	2.2	4.7
Ho	0.89	1.4	1.2	1.5	0.61	1.1	1.1	0.47	0.43	0.82
Er	2.8	4.5	3.9	5.1	2.0	3.6	3.5	1.6	1.3	2.3
Tm	0.44	0.70	0.71	0.84	0.33	0.61	0.55	0.21	0.17	0.26
Yb	3.2	4.8	5.1	6.3	2.4	4.6	4.0	1.4	1.01	1.67
Lu	0.50	0.85	0.74	1.1	0.408	0.72	0.65	0.22	0.14	0.23
Hf	0.40	1.1	0.60	1.1	0.228	0.49	0.84	0.83	0.85	4.5
Ta	0.002	0.006	0.006	0.004	0.006	0.071	0.054	1.5	0.26	6.9
Pb	<0.013	0.050	0.081	0.073	<0.013	<0.013	<0.013	0.8	0.083	2.6
Th	0.010	0.014	0.026	0.017	0.018	0.067	0.072	1.9	0.27	5.7
U	0.008	0.064	0.023	0.018	0.041	<0.004	0.033	0.40	0.060	1.3

Table 8 Calculated equilibration temperatures for host peridotite and Zone I and estimates of crystallization temperatures for Zones II+III

Sample	Type	Peridotite					Zone I					Zone II				Zone III			
		2Px (BM85)	2Px (BK90)	2Px (T98)	Ca-Opx (BK90)	Al-Opx (WS91)	2Px (BM85)	2Px (BK90)	2Px (T98)	Ca-Opx (BK90)	Al-Opx (WS91)	2Px (BM85)	2Px (BK90)	2Px (T98)	Ca-Opx (BK90)	2Px (BM85)	2Px (BK90)	2Px (T98)	Ca-Opx (BK90)
ZIN02	A	1063	1095	1024	1040	1051	1029	1074	998	1034	1090	N/A	N/A	N/A	1183	1271	1224	1352	1218
ZIN50	A	1040	1084	995	1025	1044	1056	1095	1007	1038	1054	N/A	N/A	N/A	1228	1299	1230	1397	1259
ZIN14	B	1021	1066	1010	1035	1067	1028	1074	1025	1030	1063	1184	1176	1203	1212	N/A	N/A	N/A	1245
ZIN56	B	1076	1110	1050	1048	1065	1085	1116	1061	1054	1067	N/A	N/A	N/A	1146	N/A	N/A	N/A	1210
ZIN53	C	1032	1077	996	1027	1046	1031	1074	995	1026	1047	N/A	N/A	N/A	N/A	1233	1205	1349	1238
ZIN11	*	1030	1081	985	1047	1067	N/A	N/A	N/A	N/A	N/A	N/A	N/A	N/A	N/A	N/A	N/A	N/A	N/A
ZINx8	*	1066	1097	1005	1050	1046	N/A	N/A	N/A	N/A	N/A	N/A	N/A	N/A	N/A	N/A	N/A	N/A	N/A

* samples without garnet pseudomorphs, analysed as comparative material; N/A - not analysed